CHAPTER IV
RESULTS AND DISCUSSION

Hydrogen diffusion through a carbon steel tube was investigated for various surface preparations. This study was focused on the effect of a platinum film applied to the carbon steel surface on the hydrogen diffusion through the tube. The bare carbon steel tube was taken as a reference surface before filming. Therefore two sets of experiments were conducted: one using the bare carbon steel tube and the other using the platinum-coated carbon steel tube. All tube assemblies were tested initially for leaks for two days. The hydrogen pressure reduction was then measured with time to determine the rate of mass transport of hydrogen through the tube.

4.1 Hydrogen Transport Through Carbon Steel

A series of hydrogen permeation experiments was performed using carbon steel, copper and nickel-alloy (Hastelloy-C) tubes as the diffusing material. Only a part of the carbon steel tube charged with hydrogen gas could be placed in the furnace for raising its temperature due to the temperature limitation of the pressure gauge connected close to the end. Therefore other metals that have low hydrogen diffusivity such as copper and nickel alloy (Hastelloy-C) were connected to the carbon steel tube outside the furnace in order to eliminate the effect of hydrogen diffusion occurring outside the furnace. Figure 4.1 and Figure 4.2 show the hydrogen diffusion through carbon steel, copper and nickel alloy tubes.

The leak test performed on the carbon steel tube for the first two days indicated no leak. The furnace was heated up to the set point of 345°C for 3 days. The hydrogen pressure increased from 98.0 psig to 119.5 psig during the heating up process as shown in Figure 4.1 and the average surface temperature of the carbon steel tube was 306°C. This approximates the temperature of the outlet feeder pipes in a CANDU reactor (~310°C in the CANDU-6). It can be seen that the hydrogen pressure gradually decreased by 45 psi throughout the high temperature test from 119.5 psig to 74.5 psig, in 18.1 hours.

Figure 4.2 shows that the hydrogen pressure inside the copper tube was essentially constant for 253 hours after heating. This indicates that the rate of hydrogen diffusion through copper is much less than through iron and not measurable over this time. On the other hand, the hydrogen pressure gradually decreased for the nickel-alloy tube at this temperature, indicating a measurable diffusion rate for hydrogen, the pressure decreased 45 psi, from 117.0 psig to 72.0 psig in 264 hours.

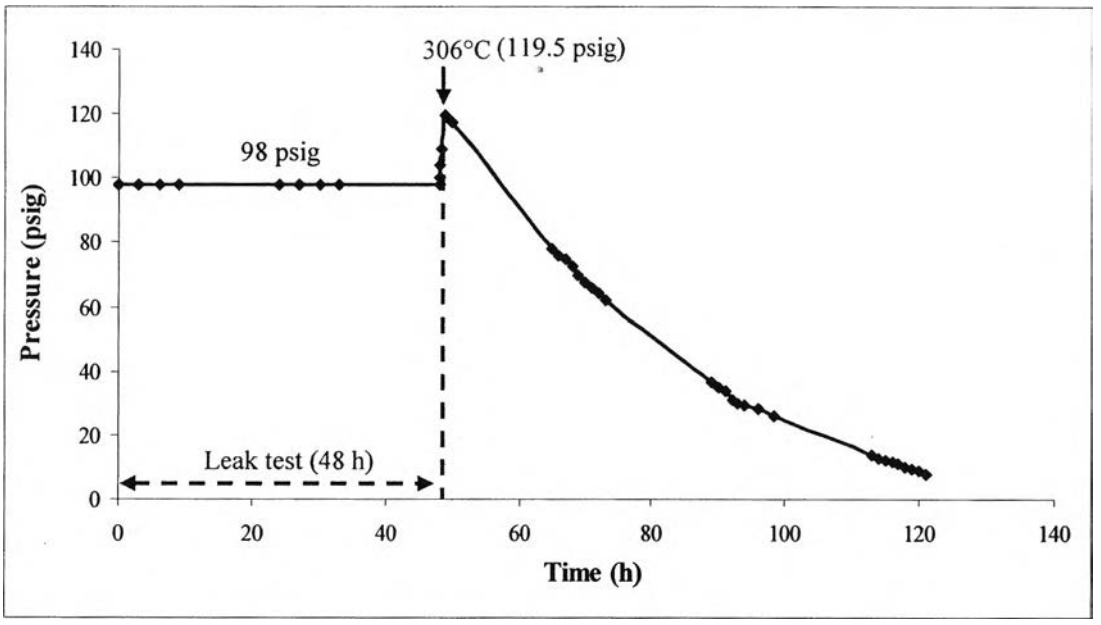

Figure 4.1 The change in hydrogen pressure inside the carbon steel tube with time (Initial hydrogen pressure: 98 psig at 25°C. Set point temperature: 345°C. Tube temperature: 306°C).

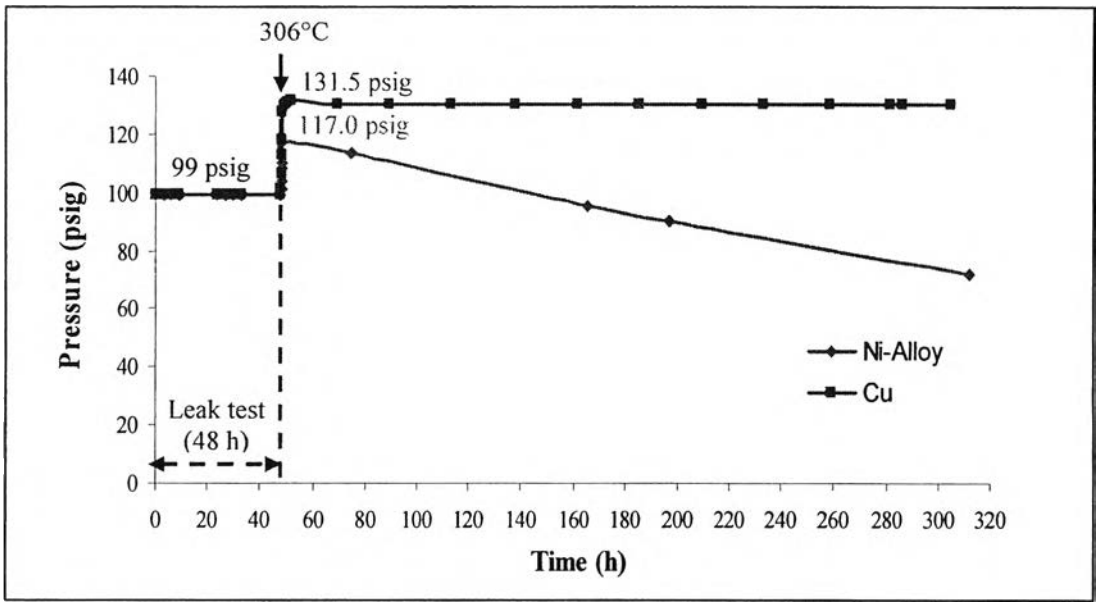

Figure 4.2 The change in hydrogen pressure inside the copper and nickel-alloy (Hastelloy-C) tube with time (Initial hydrogen pressure: 99 psig at 25°C. Set point temperature: 345°C. Tube temperature: 306°C).

Accordingly, the copper tube was chosen to prevent the hydrogen diffusion outside the furnace due to the essentially non-measurable rate for the copper tube compared to the nickel-alloy tube. Therefore, the carbon steel tube outside the furnace was r eplaced with the copper tube for subsequent hydrogen permeation experiments.

In the tube assembly containing copper, the hydrogen pressure behaved similarly to that in the earlier experiments; the hydrogen pressure gradually decreased throughout the test. However, the hydrogen diffusion rate was lower than that in the earlier experiment, as shown in Figure 4.3. This experiment was repeated. The hydrogen pressure decreased 45 psi after the heating up process, from 125.5 psig to 80.5 psig, in 47.2 hours and from 126.0 psig to 81.0 psig, in 45.5 hours for the first and the second test, respectively.

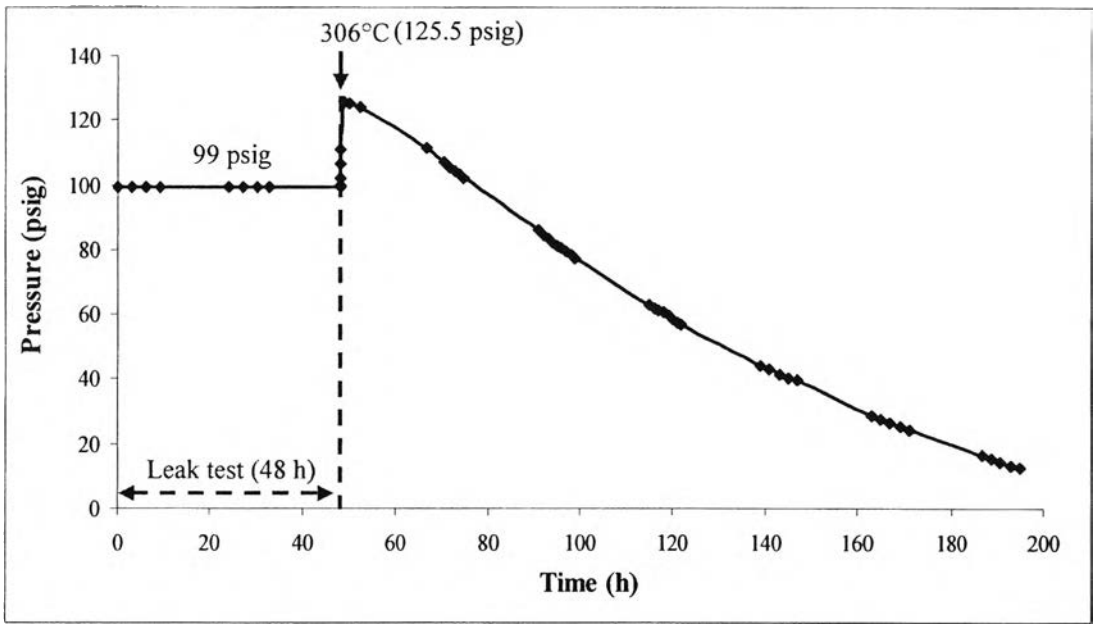

(a) Initial hydrogen pressure: 99 psig at 25°C. Set point temperature: 345°C. Tube temperature: 306°C.

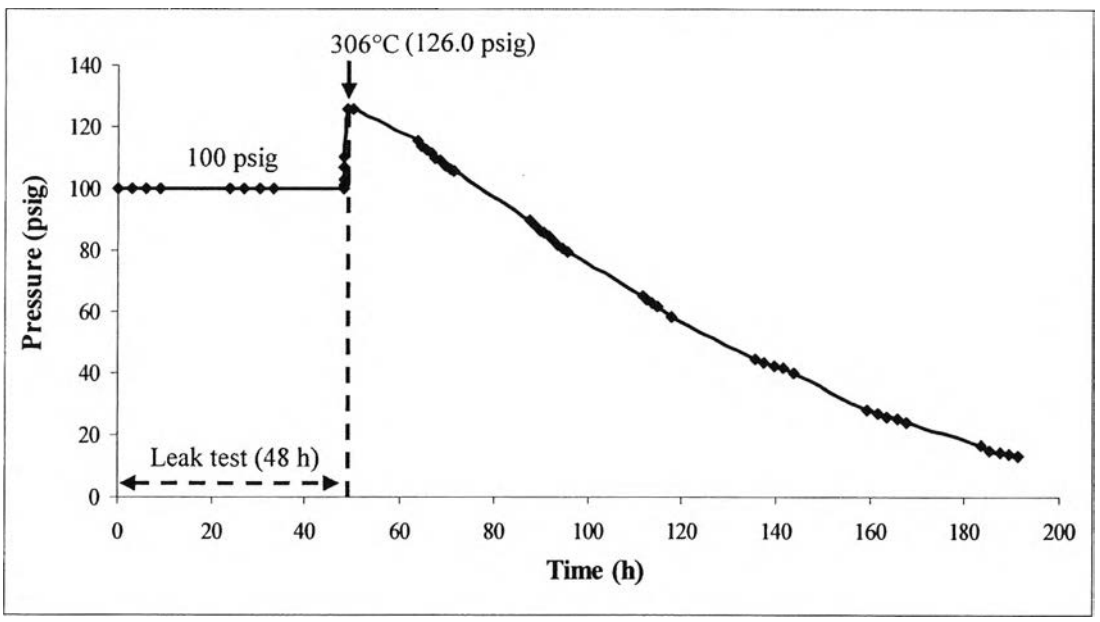

(b) Initial hydrogen pressure: 100 psig at 25°C. Set point temperature: 345°C. Tube temperature: 306°C.

Figure 4.3 The change in hydrogen pressure inside the carbon steel tube with time (the part of the carbon steel tube outside the furnace replaced with copper tube).

From the results of the first part of the hydrogen permeation experiments, it can be concluded that hydrogen pressure in the carbon steel tube decreased with time due to hydrogen diffusion at the measured temperature through the carbon steel tube only. The results are summarized in Table 4.1.

Table 4.1 Hydrogen pressure reduction (Bare, Uncoated metal)

Description	Furnace temperature (°C)	Tube temperature (°C)	Initial hydrogen pressure (psig)	Hydrogen pressure after heating (psig)	Hydrogen pressure at end of run (psig)	Time after 45 psi decrease of hydrogen pressure (h)
Carbon steel tube	345	306	98	119.5	8.00	18.130
Nickel alloy (Hastelloy-C) tube	345	306	99	117.0	72.0	263.67
Carbon steel tube outside the furnace replaced with copper tube	345 345	306 306	99 100	125.5 126.0	12.5 13.0	47.200 45.500

4.2 Effect of The Oxide Film Formed on The Outside Surface of The Carbon Steel Tube on Hydrogen Permeation

When considering the permeation of hydrogen through a carbon steel tube, Two basic processes should be considered besides diffusion in the bulk metal: the adsorption process, whereby hydrogen molecules in the gas phase dissociate on the solid surface providing adsorbed atoms which may diffuse into the solid, and the desorption process, whereby adsorbed hydrogen atoms recombine and are released as molecules. These two processes are known as surface effects and under certain conditions they may control the permeation rate (surface-limited permeation), whereas under other conditions, diffusion through the metal is the rate limiting factor (diffusion-limited permeation).

For studying the hydrogen permeation through carbon steel, a necessary requirement is that hydrogen permeation rate be controlled by diffusion in the material of the specimen not by surface effects. Oxide films, usually present on a metal surface, lower the degree of hydrogen dissociation and recombination on the inside and outside surfaces, respectively. Significant reductions in the hydrogen permeation rate are achieved even with very thin oxide films. The removal of the oxide surface layer that retards the hydrogen passage from the specimen is a necessary condition for hydrogen diffusivity measurement in metal.

This study also performed experiments to prove that oxidized or contaminated surfaces affected the measured permeation. A similar experiment was performed; 100 psig of hydrogen gas was heated up with the set point temperature of the furnace at 310°C for 6 days. Figure 4.4 shows the qualitative analysis of hydrogen permeation through carbon steel tube with and without oxide film. Hydrogen pressure values shown are not precise due to the malfunctioned pressure gauge. The hydrogen pressure after heating was higher than the calculated hydrogen pressure after heating. The hydrogen pressure increased from 100 psig to 135 psig during the heating up process and the average surface temperature of the carbon steel tube was 277°C. After 2 days of heating, the tube was taken out of the furnace and quickly polished with 600 grit of sandpaper to remove the oxide film formed on the

outside surface. The tube was sanded to a metallic finish in about 3 minutes and then replaced in the furnace. The hydrogen pressure after the removal of the oxide film dropped rapidly from 105 to 85 psig as shown in Figure 4.4. This is presumably because there was no oxide film to act as a barrier to hydrogen diffusion. However, the hydrogen pressure might drop below 105 psig during the removal and sanding at room temperature before replacement in the furnace and the hydrogen pressure then increased to 105 psig at high temperature.

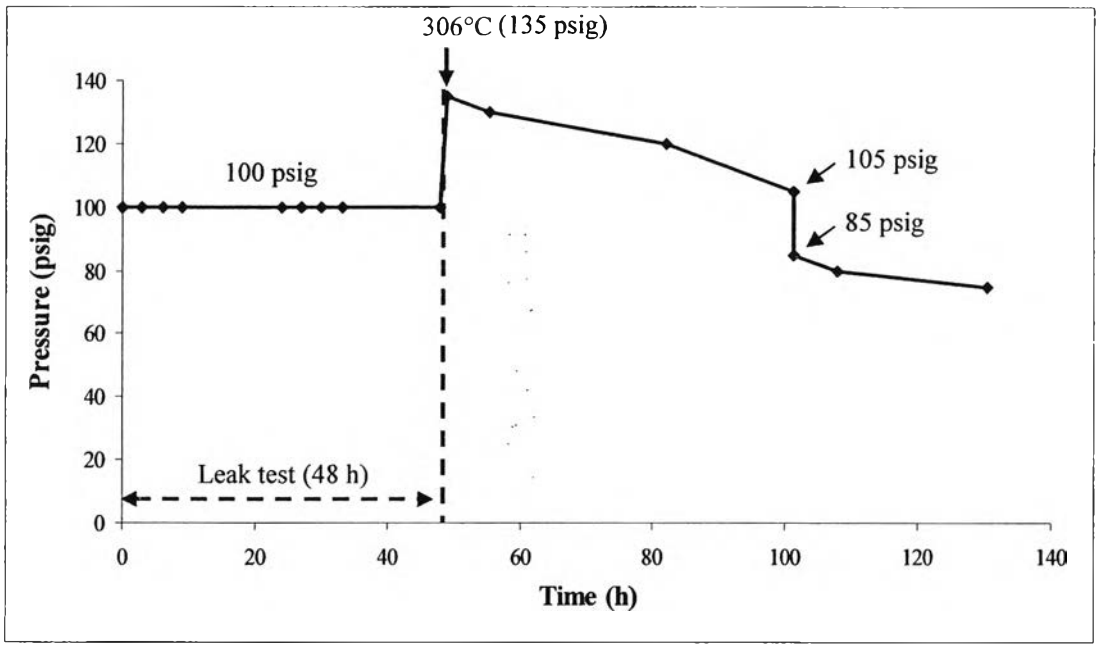

Figure 4.4 The change in hydrogen pressure inside the carbon steel tube with time after the removal of the oxide film formed on the outside surface (Initial hydrogen pressure: 100 psig at 25°C. Set point temperature: 310°C. Tube temperature: 306°C).

Since platinum is a known catalyst for hydrogen association/dissociation reactions, it was deposited on the tube surfaces to see if it would affect the permeation results. It was also possible that the steel oxidation could be affected by platinum deposition and that could affect the measurements.

4.3 Coating Platinum on Carbon Steel Surfaces

Platinum films deposited on the carbon steel tube surface were evaluated by both visual inspection and surface characterization techniques. A Field Emission Scanning Electron Microscopy (FESEM) was used to examine the morphology of the platinum films. Energy Dispersive Spectrometry (EDS) was used to verify the deposition of the platinum. X-Ray Diffraction and Raman Spectroscopy were also used.

4.3.1 Visual Inspection

The preliminary characterization was done by visual inspection and photography to determine the uniformity and the color of platinum films deposited on the surface of carbon steel ASTM A179.

Figure 4.5 shows photographs of a number of samples. It can be seen that there was no obvious oxide layer on the inside or outside surface of the bare carbon steel. There was a significant difference between the tube surface before and after filming. The surface of the original metal was smoother than the surface of the sample after the film was formed. The platinum films formed on both the inside and outside surfaces of the carbon steel are metallic gray similar to the color of the bare carbon steel surface.

The inside surface of carbon steel tube seemed to have some oxide film on the surface after filming, Figure 4.5c. There were some brownish orange spots. Comparison with the standard iron oxides color (Cornell, 2003), Figure A (in Appendix A), suggested that these brownish orange spots were haematite. However, this was only a preliminary observation based on the observation by eye. It had to be confirmed by other surface characterizing techniques.

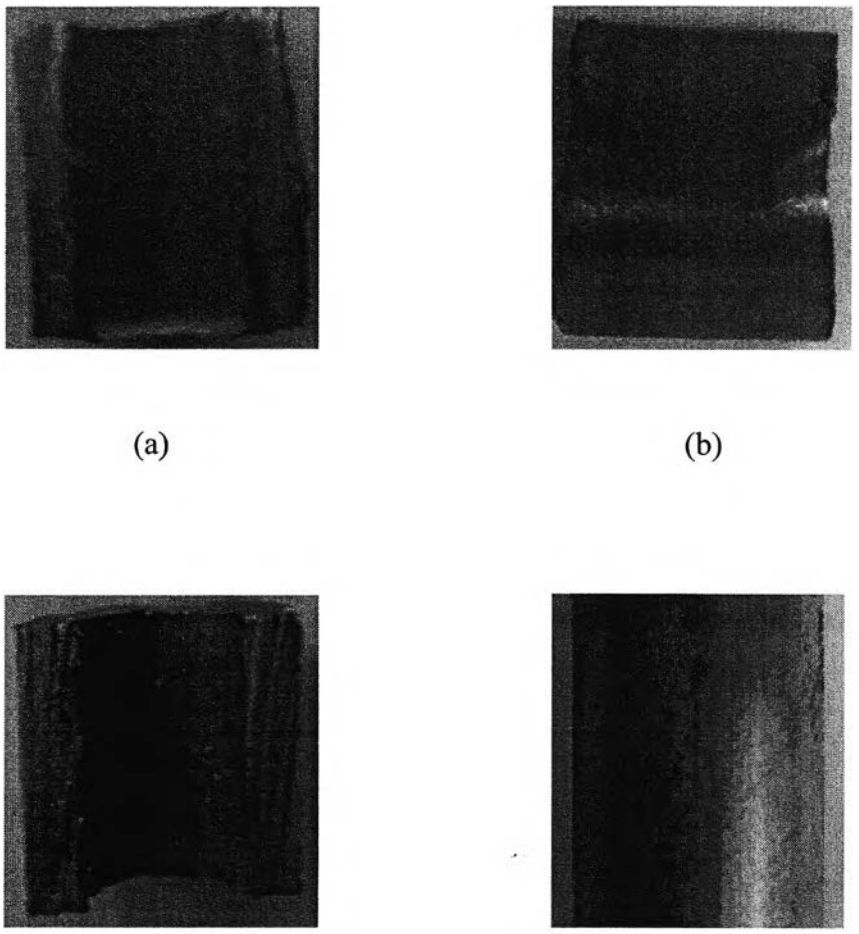

Figure 4.5 Visual photographs of samples (a) inside surface of bare carbon steel (b) outside surface of bare carbon steel (c) platinum film formed on the inside surface of carbon steel tube (d) platinum film formed on the outside surface of carbon steel tube.

4.3.2 Field Emission Scanning Electron Microscopy (FESEM)

The platinum films were characterized with the FESEM technique. In this study, there are two results obtained by using this technique which are FESEM surface micrographs and Energy Dispersive X-Ray Analysis (EDX) data.

4.3.2.1 FESEM Micrographs

FESEM micrographs of the surface were taken. The coating of platinum on the inside and outside surfaces is concurrently discussed because of the same operating conditions.

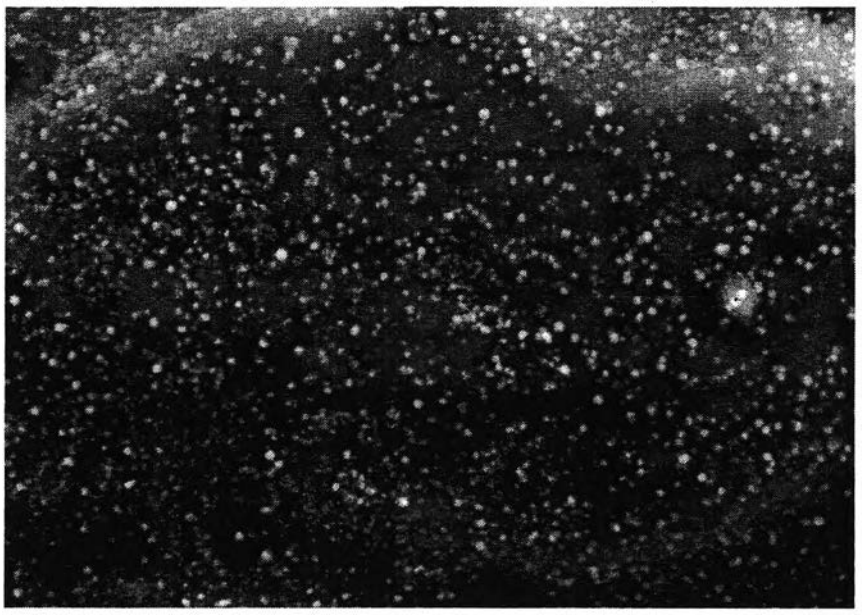

(a)

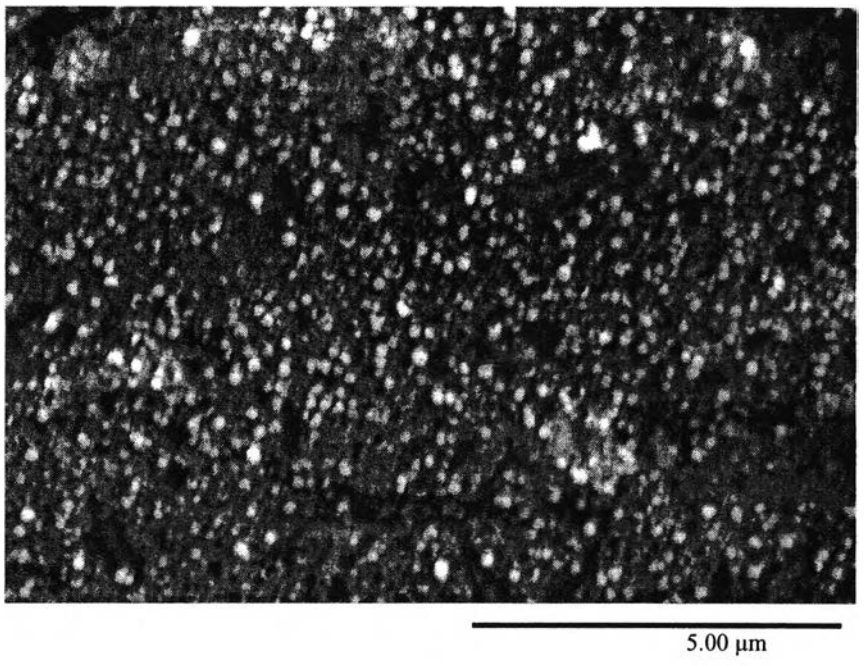

(b)

Figure 4.6 FESEM surface micrographs of platinum film formed on the surfaces of carbon steel at 11000X magnifications (a) inside surface of carbon steel tube (b) outside surface of carbon steel tube.

Figure 4.6 shows the FESEM surface micrograph of the platinum film formed on the inside and outside surface of the carbon steel tube. The platinum was present as discrete particles that did not totally cover the steels. It just nucleated platinum from solution-probably as single crystallites.

Figure 4.7 shows the platinum film morphology at higher resolution, 60000X magnifications. The uniformity and structure of the platinum particles on the inside and outside surface of the carbon steel tube can be seen in Figure 4.7a and Figure 4.7b, respectively. Apparently, the platinum particles which coated both the inside and outside surface were quite similar in their overlay.

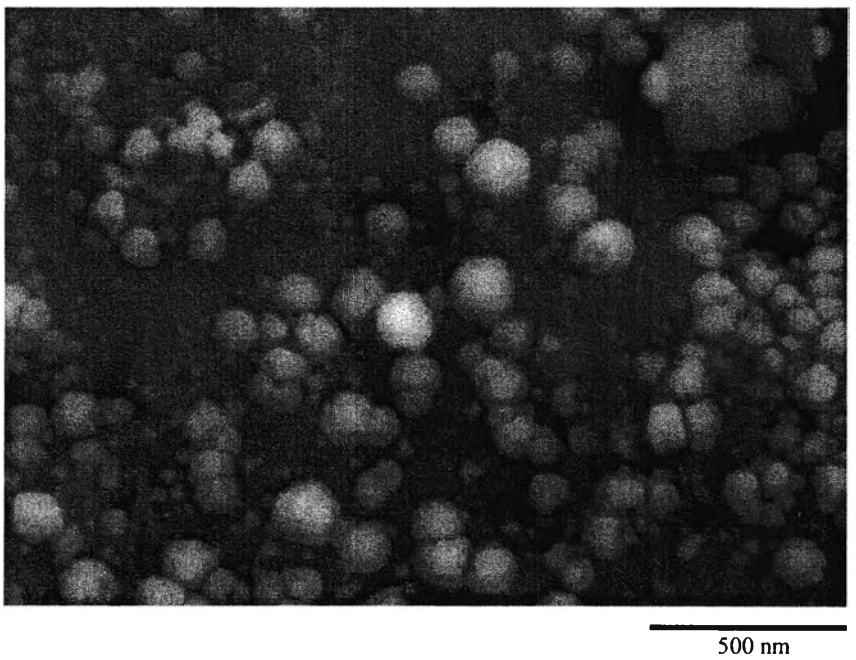

(a)

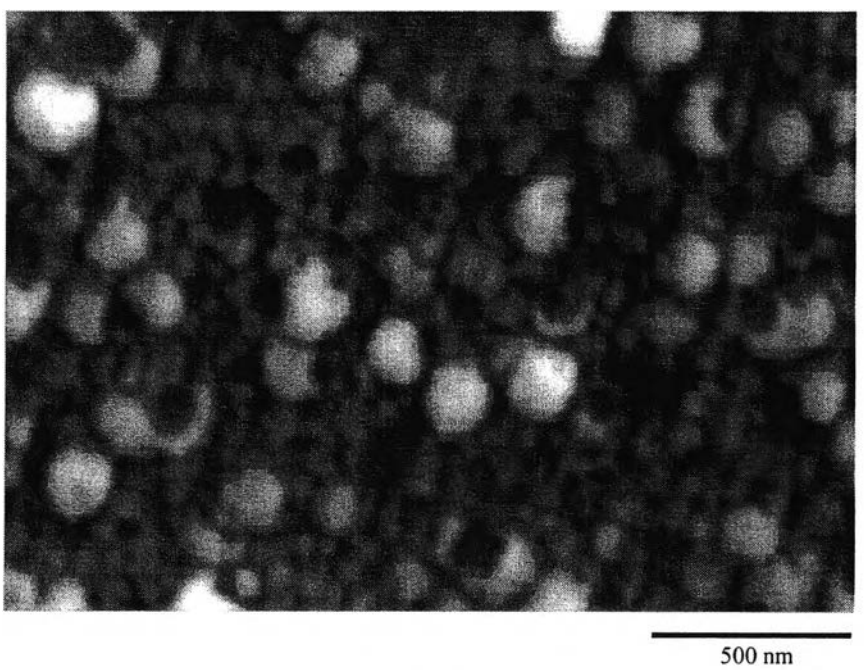

(b)

Figure 4.7 FESEM surface micrographs of platinum film formed on the inside and outside surfaces of carbon steel tube at 60000X magnifications (a) inside surface (b) outside surface.

4.3.2.2 Energy Dispersive X-Ray Analysis (EDX)

Elemental analyses of the platinum films on both the inside and outside surfaces were obtained by using EDS coupled with FESEM micrographs in order to select the area of interest.

4.3.2.2.1 Bare Carbon Steel Tube

Figure 4.8 illustrates the selected area of the carbon steel that was used for EDX analysis. The elemental analyses for uncoated carbon steel are shown in Table 4.2. It can be seen that the bare carbon steel mainly consisted of iron (Fe) with small amounts of carbon (C), phosphorous (P) and chromium (Cr). The amounts of other elements such as sulfur (S) were low, less than the detection limit of 0.04%wt.

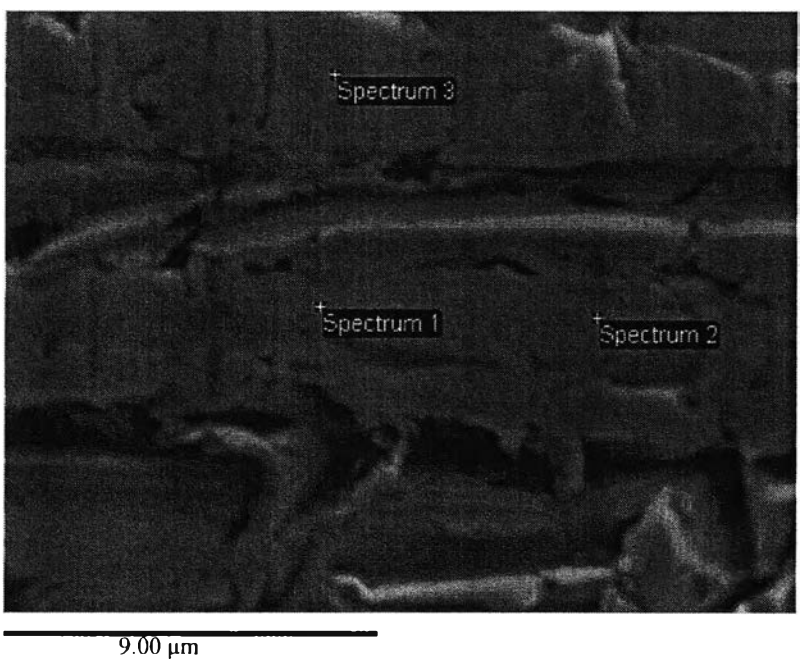

Figure 4.8 Selected area of bare carbon steel sample for EDX analysis; FESEM micrograph at 11000X magnification.

Table 4.2 Elemental analysis of bare carbon steel

Selected Area	Element (Weight %)				
	Fe	**C**	**P**	**Cr**	**Total**
Spectrum 1	95.48	3.88	0.55	0.09	100
Spectrum 2	96.20	3.08	0.57	0.15	100
Spectrum 3	95.48	3.76	0.63	0.13	100
Mean	95.72	3.57	0.58	0.13	100

4.3.2.2.2 Platinum-Coated Carbon Steel Tube

The selected areas of the inside and outside surfaces coated with platinum are shown in Figure 4.9 and Figure 4.10. From EDX analysis, the main component was iron (Fe) along with (Pt). The concentration of other components (Tables B1 and B2) was low. The platinum concentration on the inside and outside surfaces was in the range of 3.41-17.46 weight % and 14.68-27.79 weight%, respectively. It can be seen that the platinum concentration on the inside surface was lower than that on the outside surface, probably because of the different methods of coating. The particulate nature of the platinum is clear.

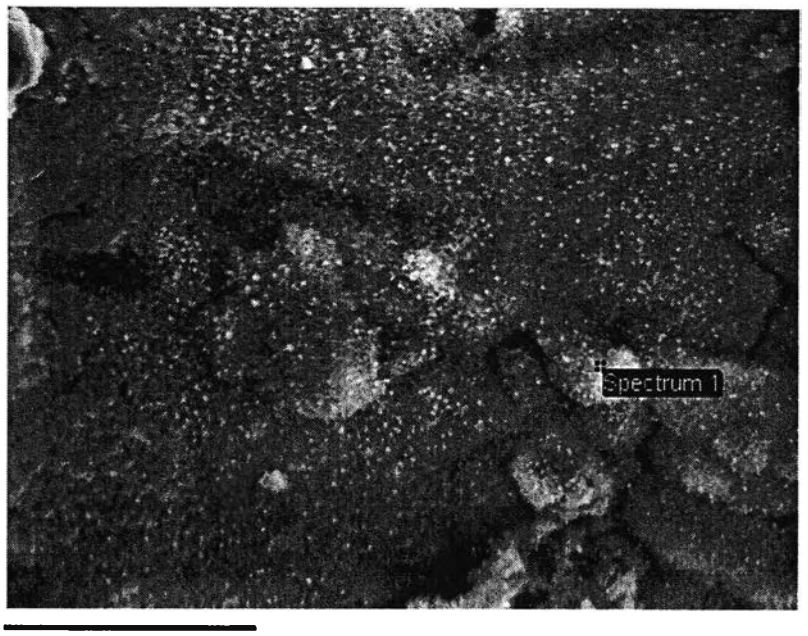

(a)

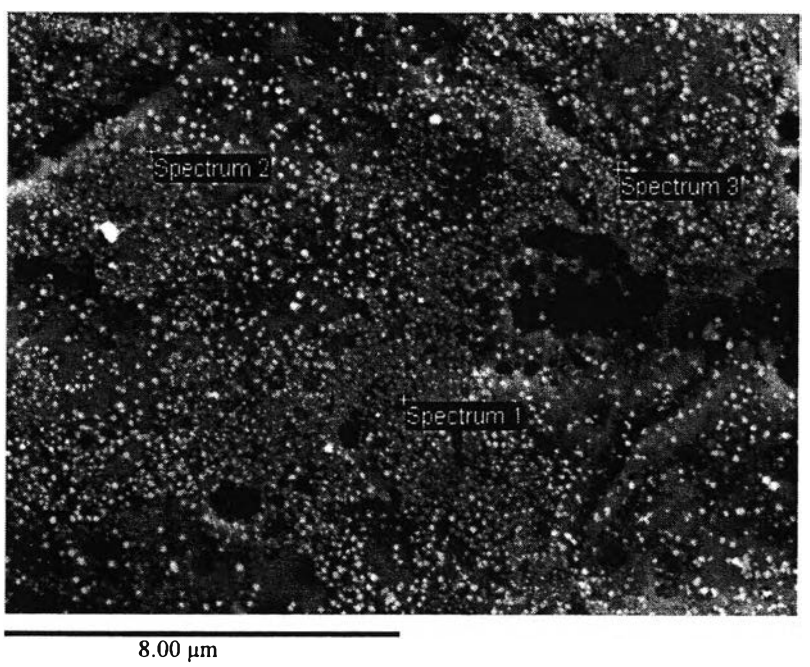

(b)

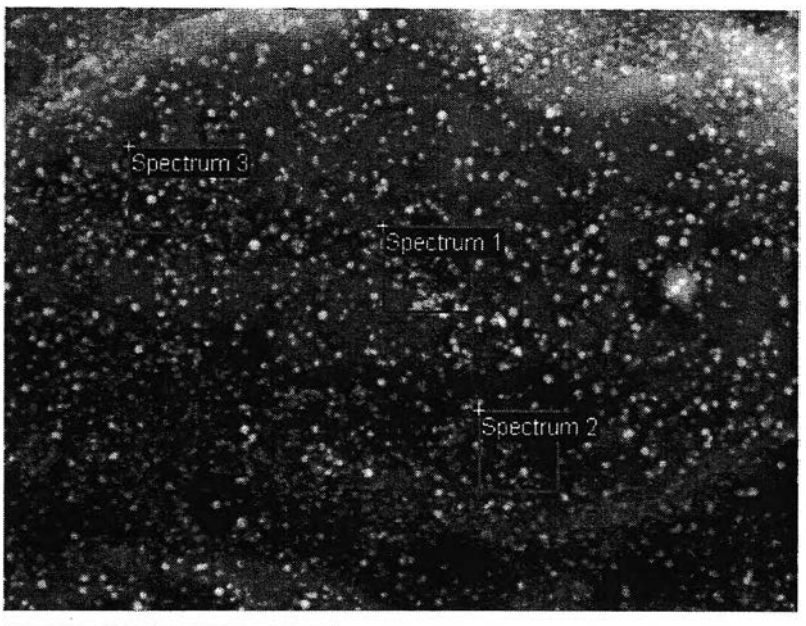

(c)

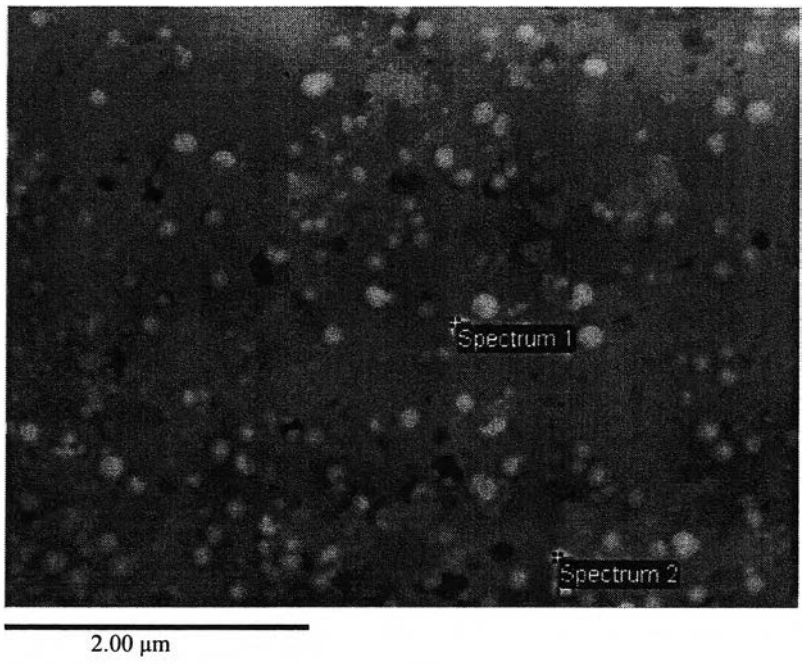

(d)

Figure 4.9 Selected platinum film areas of the inside carbon steel surface coated with platinum for EDS analysis: FESEM micrographs, (a)-(d) the selected areas of the inside surfaces coated with platinum at different positions.

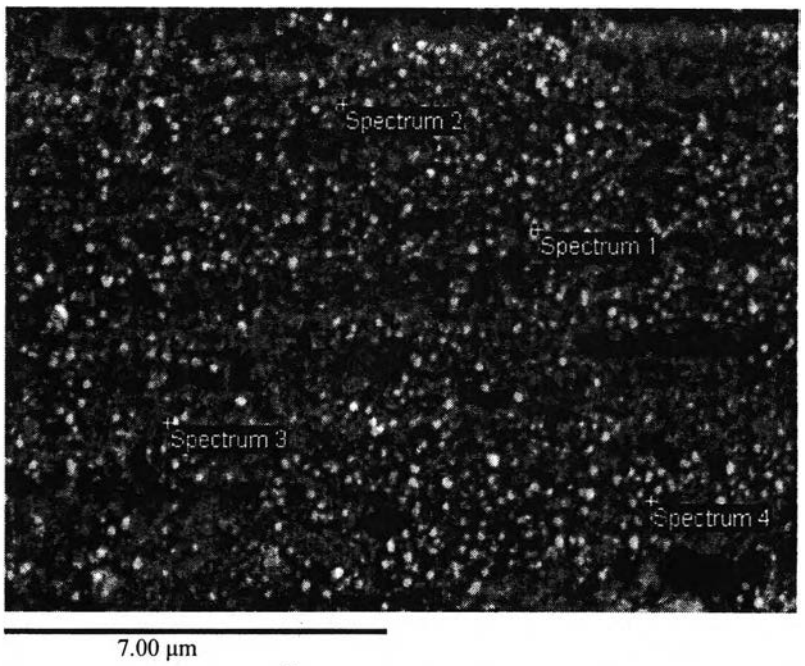

(a)

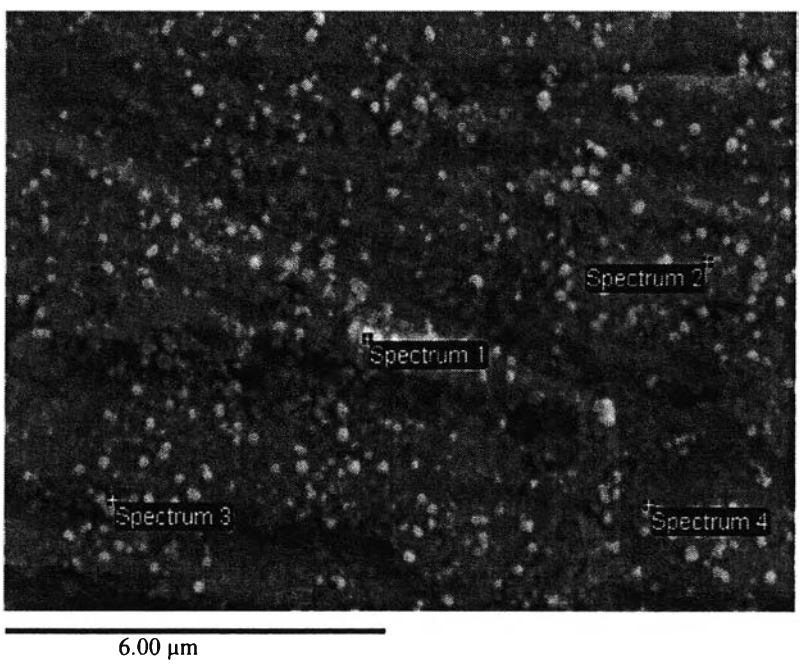

(b)

Figure 4.10 Selected areas of the outside carbon steel surface coated with platinum for EDS analysis: FESEM micrographs, (a)-(b) the selected areas of the outside surfaces coated with platinum at different positions.

By normalizing the concentration of iron (Fe) relative to oxygen (O) for the inside surface, the crystal structure of the oxide formed on the surface could be roughly determined. Because the oxide could be haematite (Fe_2O_3), the concentration of oxygen was set to 3. Table 4.3 shows the ratio of Fe to O concentration corresponding molar proportion of Fe, which was >2. This is because the EDX beam would pick up an interference signal from the underlying steel matrix that mainly consisted of Fe. The crystal structure of the oxide was analyzed by using another technique.

Table 4.3 Normalized concentration of Fe to O (platinum-coated inside surface of the carbon steel)

Description	Fraction (Weight %)		Fraction (Mol %)		Normalized to O	
	Fe	O	Fe	O	Fe	O
Figure 4.9a						
Spectrum 1	65.65	22.22	0.401	0.474	2.54	3.00
Figure 4.9b						
Spectrum 1	65.90	21.91	0.430	0.499	2.59	3.00
Spectrum 2	94.71	-	0.972	-	-	-
Spectrum 3	78.59	-	0.792	-	-	-
Figure 4.9c						
Spectrum 1	91.59	-	0.882	-	-	-
Spectrum 2	70.55	23.17	0.441	0.505	2.62	3.00
Spectrum 3	93.71	-	0.888	-	-	-
Figure 4.9d						
Spectrum 1	93.10	-	0.844	-	-	-
Spectrum 2	94.65	-	0.792	-	-	-

Trace amounts of sodium (Na) and (Cl) were found on the platinum-coated inside and outside surfaces of the carbon steel tube, probably from the sodium hydroxide and chloroplatinic acid which were used for the coating. The presence of sodium and chlorine precipitated sodium chloride, (NaCl), as mentioned in the literature. However, as shown in Table 4.4 and Table 4.5, the ratio of sodium to chloride was much greater than 1, probably because excess sodium hydroxide was used in the deposition.

Table 4.4 Normalized concentration of Na to Cl (platinum-coated inside surface of the carbon steel)

Description	Fraction (Weight %)		Fraction (Mol %)		Normalized to Cl	
	Na	Cl	Na	Cl	Na	Cl
Figure 4.9a						
Spectrum 1	1.51	0.25	0.0224	0.00241	9.31	1.00
Figure 4.9b						
Spectrum 1	0.42	0.03	0.00666	0.00113	5.88	1.00
Spectrum 2	0.48	0.16	0.0120	0.00259	4.62	1.00
Spectrum 3	0.85	0.27	0.0208	0.00429	4.85	1.00
Figure 4.9c						
Spectrum 1	0.51	0.14	0.0119	0.00213	5.61	1.00
Spectrum 2	0.28	0.05	0.00425	0.000492	8.63	1.00
Spectrum 3	0.42	0.13	0.00966	0.00194	4.98	1.00
Figure 4.9d						
Spectrum 1	-	-	-	-	-	-
Spectrum 2	-	-	-	-	-	-

Table 4.5 Normalized concentration of Na to Cl (platinum-coated outside surface of the carbon steel)

Description	Fraction (Weight %)		Fraction (Mol %)		Normalized to Cl	
	Na	Cl	Na	Cl	Na	Cl
Figure 4.10 a						
Spectrum 1	0.4	0.08	0.0120	0.00156	7.71	1.00
Spectrum 2	0.42	0.14	0.0101	0.00220	4.62	1.00
Spectrum 3	0.33	0.07	0.00789	0.00109	7.27	1.00
Spectrum 4	-	-	-	-		-
Figure 4.10 b						
Spectrum 1	1.09	0.31	0.0387	0.00716	5.42	1.00
Spectrum 2	0.60	0.19	0.0161	0.00331	4.87	1.00
Spectrum 3	0.50	0.17	0.0132	0.00291	4.53	1.00
Spectrum 4	1.14	0.30	0.0299	0.00511	5.86	1.00

4.3.3 X-Ray Diffraction

The XRD spectrum for the platinum-filmed carbon steel is shown in Figure 4.11. It displays four main peaks at 2θ of 40.04°, 44.70°, 65.12°and 82.48°. From comparison with the reference iron and platinum metal spectra it was found that the first broad peak at 2θ of 40.04° corresponds to platinum metal. However the absence of the remaining peaks of platinum metal might be caused by the small amount of platinum deposited. The peaks at 2θ of 44.70°, 65.12°and 82.48° coincide with the spectrum of iron metal, the main component in carbon steel. Meanwhile the spectra from the various platinum oxides were overlaid on this pattern and none of them corresponded to the peaks in this pattern. Therefore it can be concluded that the platinum formed on the carbon steel surface was pure platinum metal.

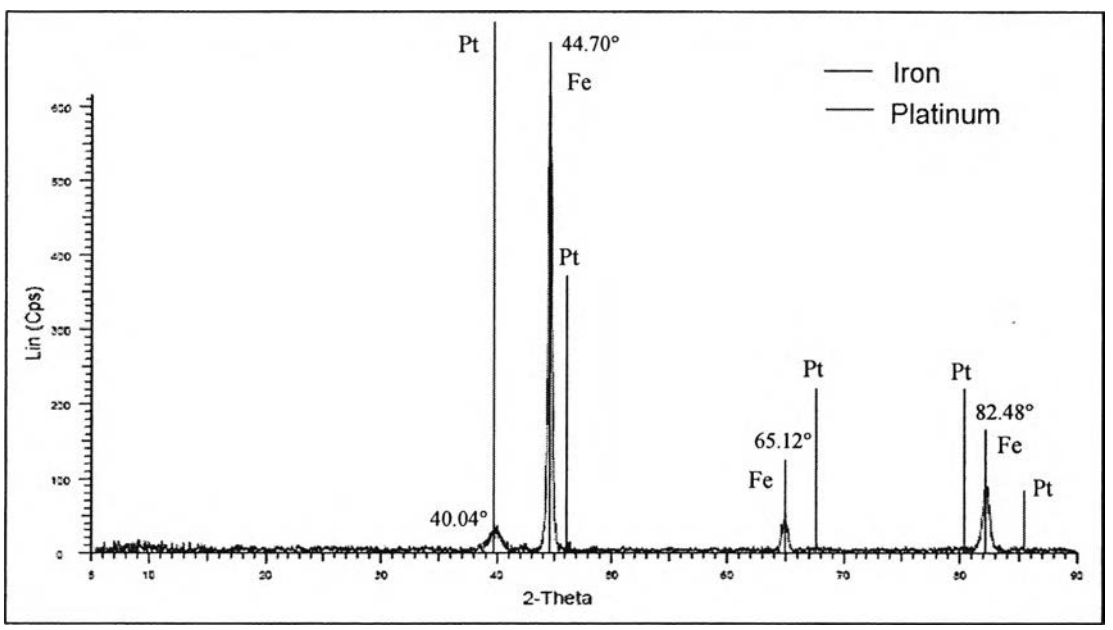

Figure 4.11 X-ray diffraction spectrum of platinum-filmed carbon steel compared with reference spectra of iron and platinum.

4.3.4 Raman Spectroscopy

The chemical structure of any oxide formed on the inside surface of the carbon steel can be identified by Raman Spectroscopy. Two spectra were obtained: the first was from bare carbon steel and the second from oxide formed on the inside surface of the platinum-coated carbon steel tube as shown in Figure 4.12 and Figure 4.13, respectively. It can be seen that the spectrum of bare carbon steel shows no peak over the Raman shift range shown in Figure 4.12, while the Raman spectrum of oxide on the coated surface shows seven main peaks at 285.86cm^{-1}, 400.37 cm^{-1}, 492.91 cm^{-1}, 591.46 cm^{-1}, 640.18 cm^{-1}, 783.18 cm^{-1} and 1,290.45 cm^{-1}.

By comparison with the reference haematite spectrum data (Table C in Appendix C), it can be concluded that the oxide mainly consisted of haematite formed after or during coating because of the absence of the peak in the speatra of bare carbon steel. Due to trace amounts of other contaminants in the platinum films, the position of the peak could be shifted from the reference position.

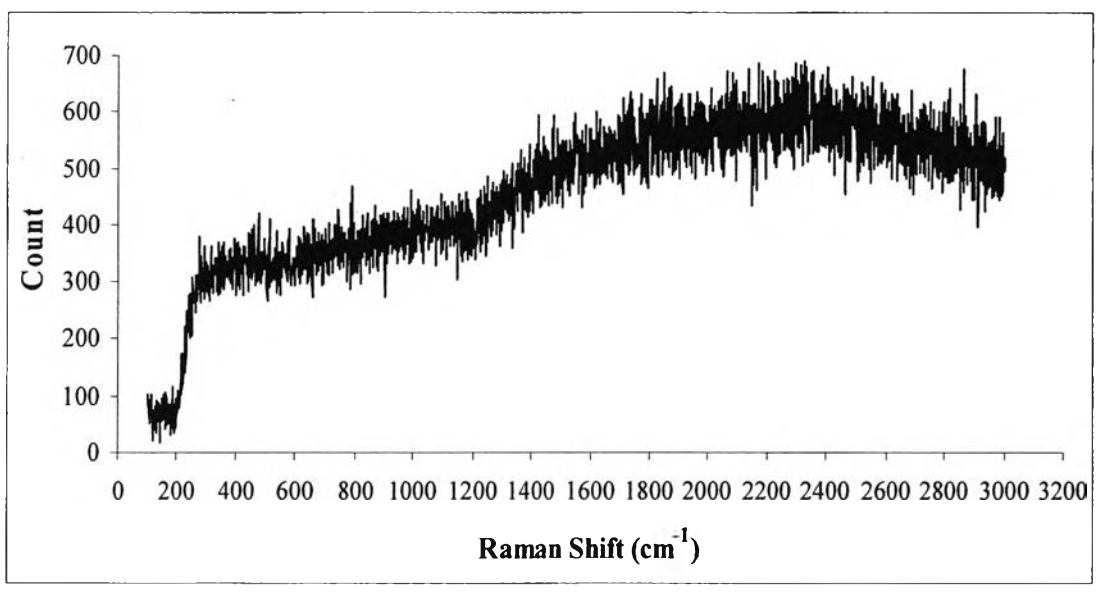

Figure 4.12 Raman spectrum of bare carbon steel.

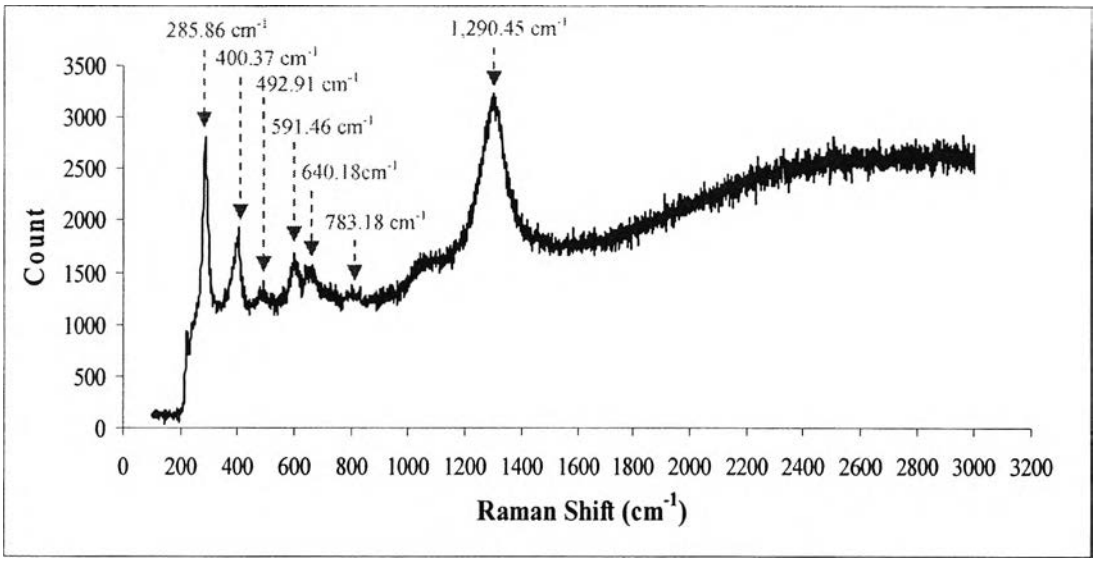

Figure 4.13 Raman spectrum of oxide on the platinum-coated inner surface of carbon steel tube.

4.4Kinetic surface bar rier to hydrogen mass transfer

It is assumed that the resistance of the platinum layer itself to ingress of hydrogen into the steel is small because of the discrete nature of the particles. In fact, the platinum should serve to catalyze the dissociation of molecular hydrogen and increase the ingress. All experiments in this section were repeated once and the average hydrogen diffusivity values reported.

4.4.1 Hydrogen Diffusion With Platinum Coated on The Inside Surface of Carbon Steel Tube

Figure 4.14a and Figure 4.14b show the hydrogen diffusion through the carbon steel tube coated with platinum on the inside surface. Both tests were performed at 345°C as the set point temperature of the furnace, giving a measured surface temperature of 306°C. The hydrogen pressure decreased from 125.0 psig to 12.5 psig in 295 minutes in the first test and from 123.0 psig to 12.5 psig in 320 minutes in the second test. This increase in hydrogen diffusion rate over that

measured for the uncoated tube indicates that the platinum reduces surface effects experienced in previous experiments.

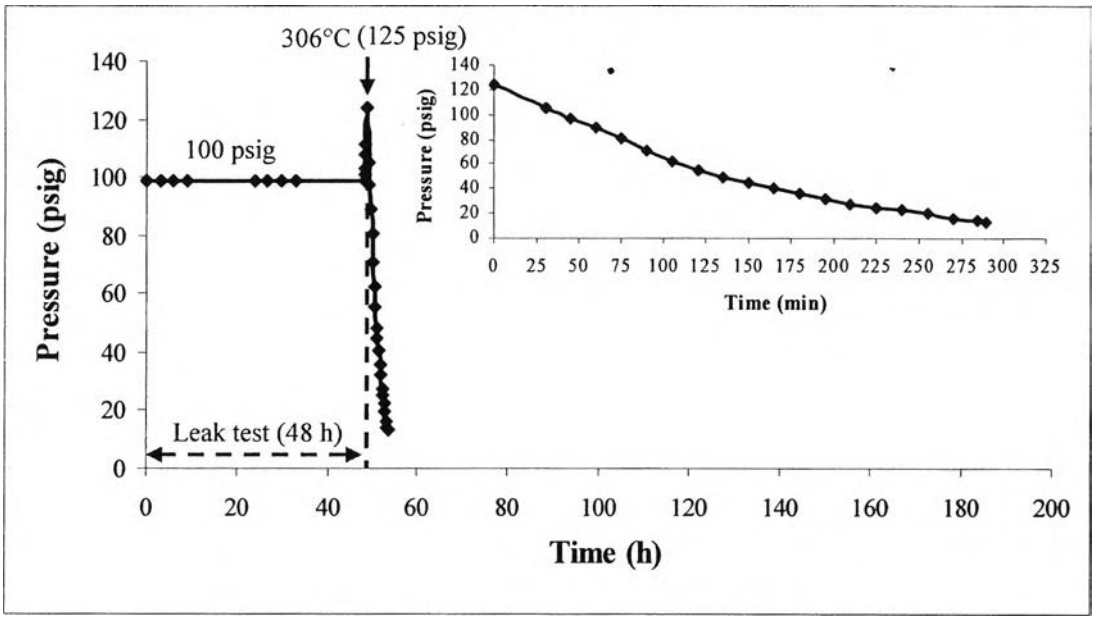

(a) Initial hydrogen pressure: 100 psig at 25°C. Set point temperature: 345°C. Tube temperature: 306°C.

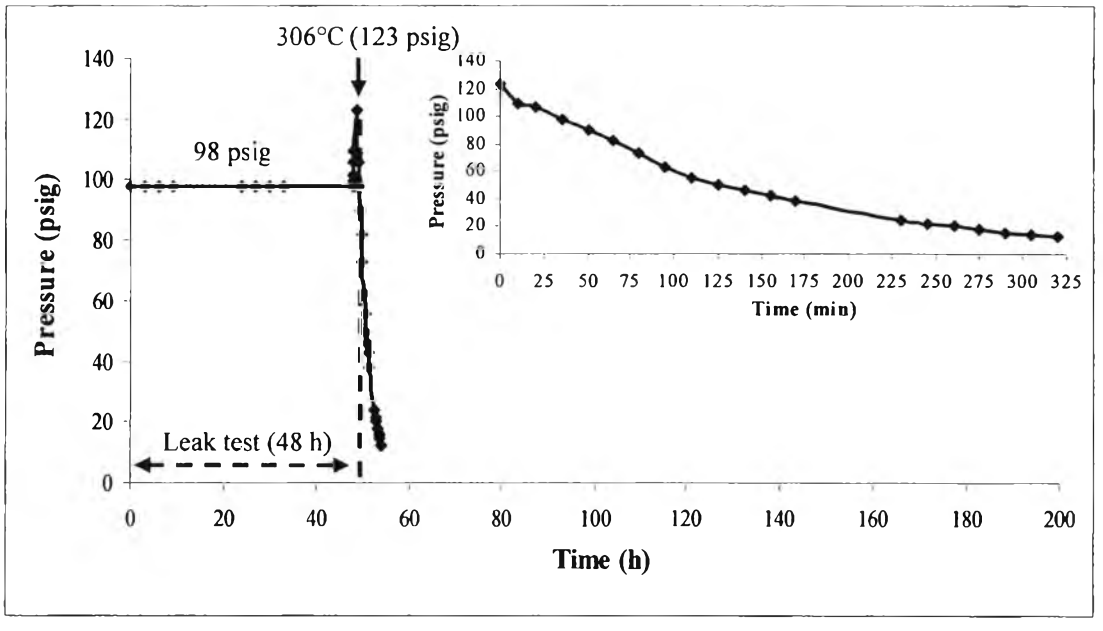

(b) Initial hydrogen pressure: 98 psig at 25°C. Set point temperature: 345°C. Tube temperature: 306°C.

Figure 4.14 The change in hydrogen pressure inside the filmed carbon steel tube with time (platinum on the inside surface of carbon steel tube).

4.4.2 Hydrogen Diffusion With Platinum Coated on The Outside Surface of Carbon Steel Tube

Two experiments were performed with carbon steel tube coated with platinum on the outside surface, Figure 4.15. The behavior of hydrogen pressure was similarly to that in the previous tests, the hydrogen pressure gradually decreased. The hydrogen pressure decreased from 124.0 psig to 13.5 psig in 290 minutes and in 310 minutes for the first and the second test, respectively, with the surface temperature of the tube at 306°C. The results indicate that the platinum reduced the resistance on the outside of the tube also.

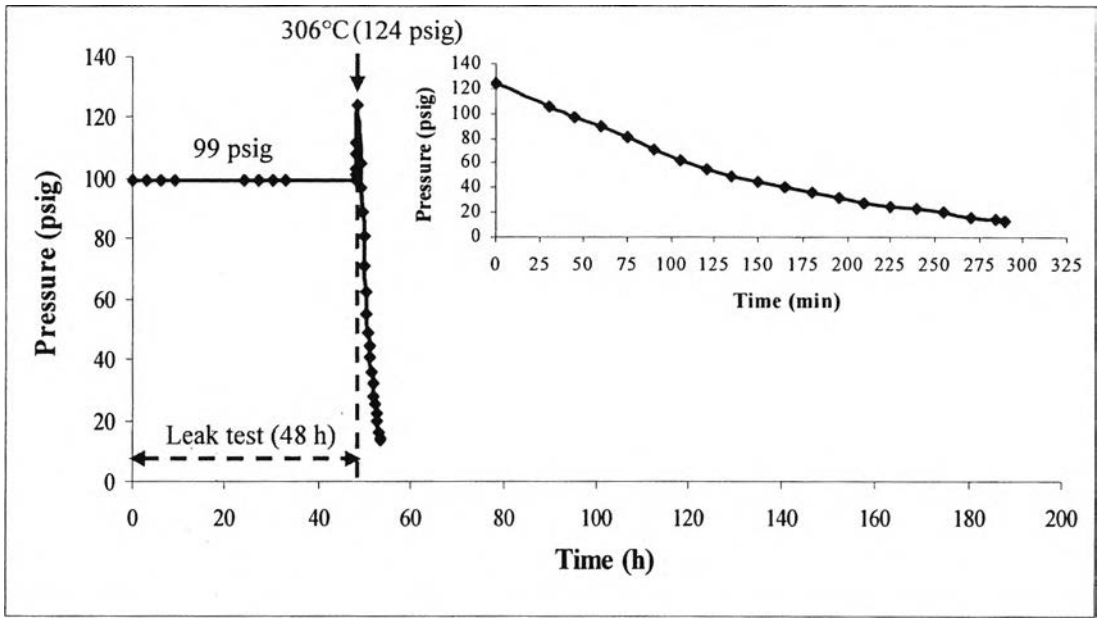

(a) Initial hydrogen pressure: 99 psig at 25°C. Set point temperature: 345°C. Tube temperature: 306°C.

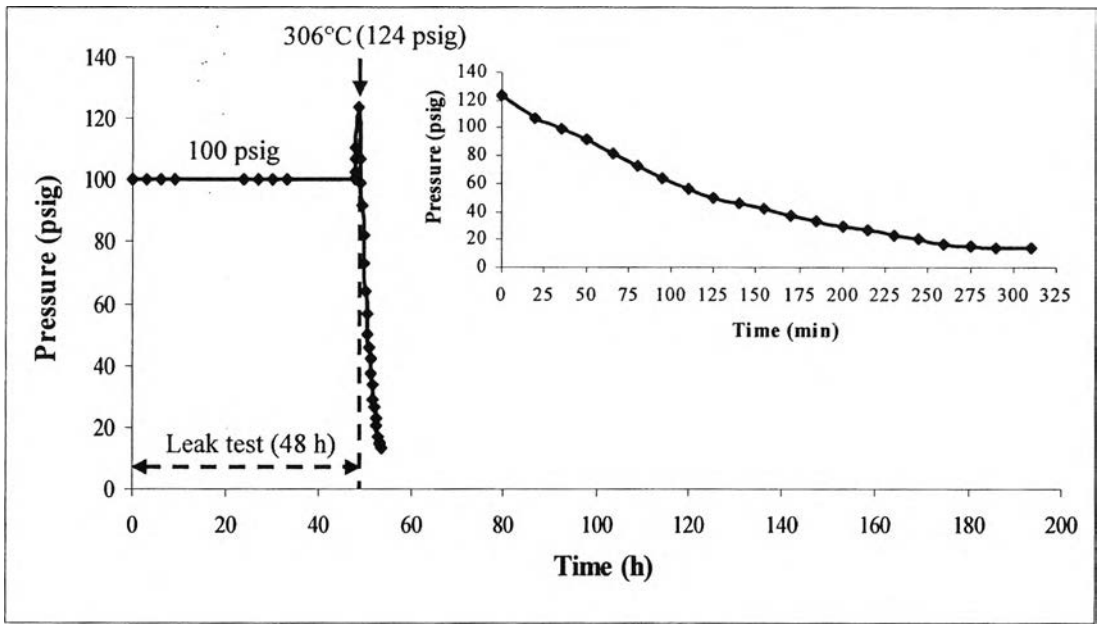

(b) Initial hydrogen pressure: 100 psig at 25°C. Set point temperature: 345°C. Tube temperature: 306°C

Figure 4.15 The change in hydrogen pressure inside the filmed carbon steel tube with time (platinum on the outside surface of carbon steel tube).

4.4.3 Hydrogen Diffusion With Platinum Coated on Both Inside and Outside Surfaces of Carbon Steel Tube

In this section, platinum was coated on both the inside and outside surface of the carbon steel tube so that the data obtained could be related to hydrogen diffusion limited only by resistance in the bulk metal. Measurements were done with the tube in the temperature range of 180-360°C.

Figures 4.16-4.19 show the hydrogen pressure reduction with time measured at the various temperatures.

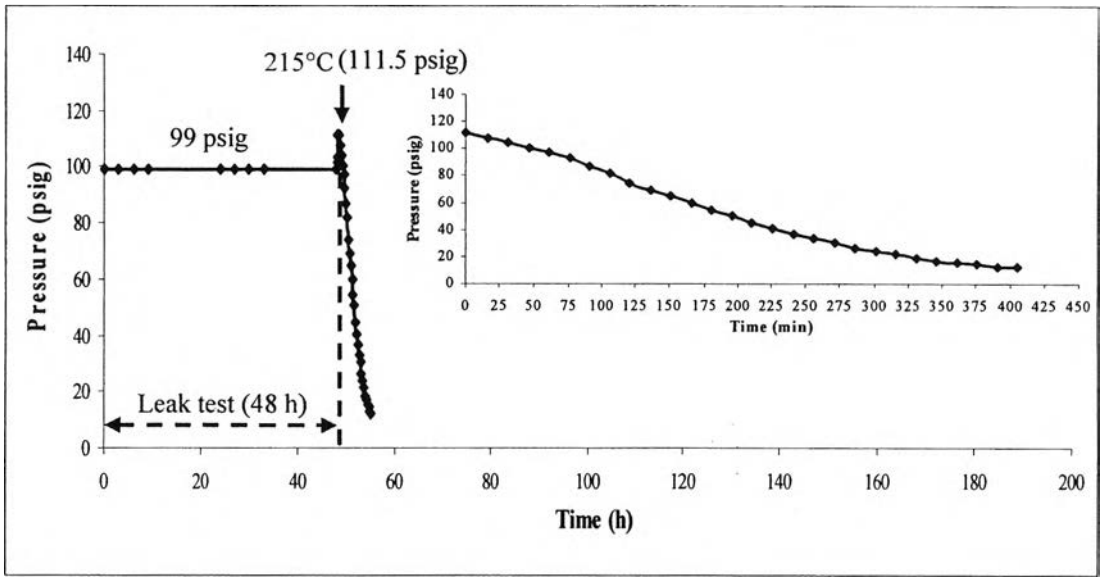

(a) Initial hydrogen pressure: 99 psig at 25°C. Set point temperature: 215°C. Tube temperature: 180°C.

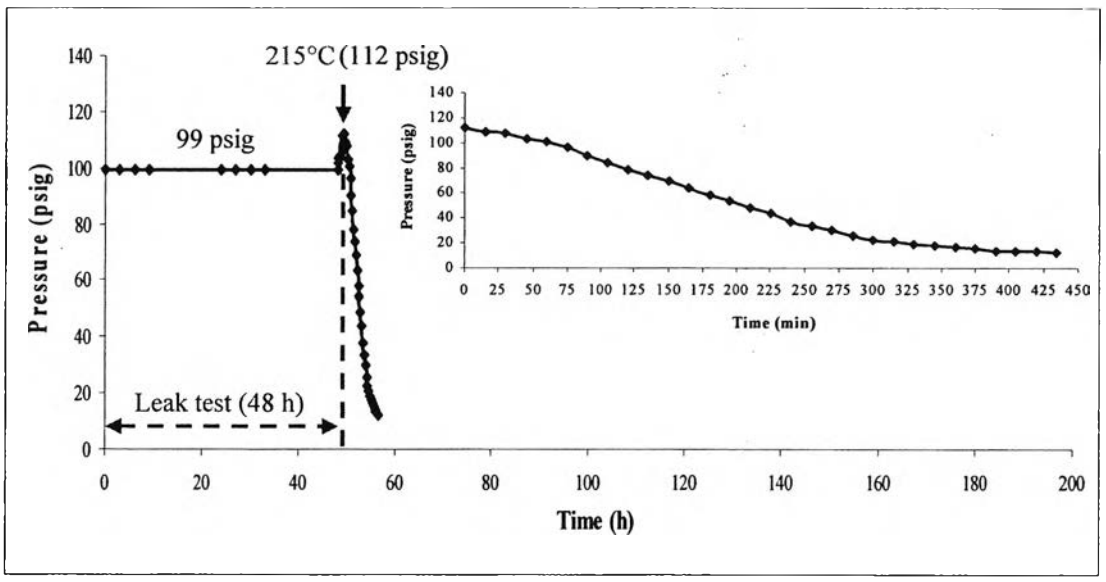

(b) Initial hydrogen pressure: 99 psig at 25°C. Set point temperature: 215°C. Tube temperature: 180°C.

Figure 4.16 The change in hydrogen pressure inside the filmed carbon steel tube with time (platinum on both the inside and outside surfaces of carbon steel tube).

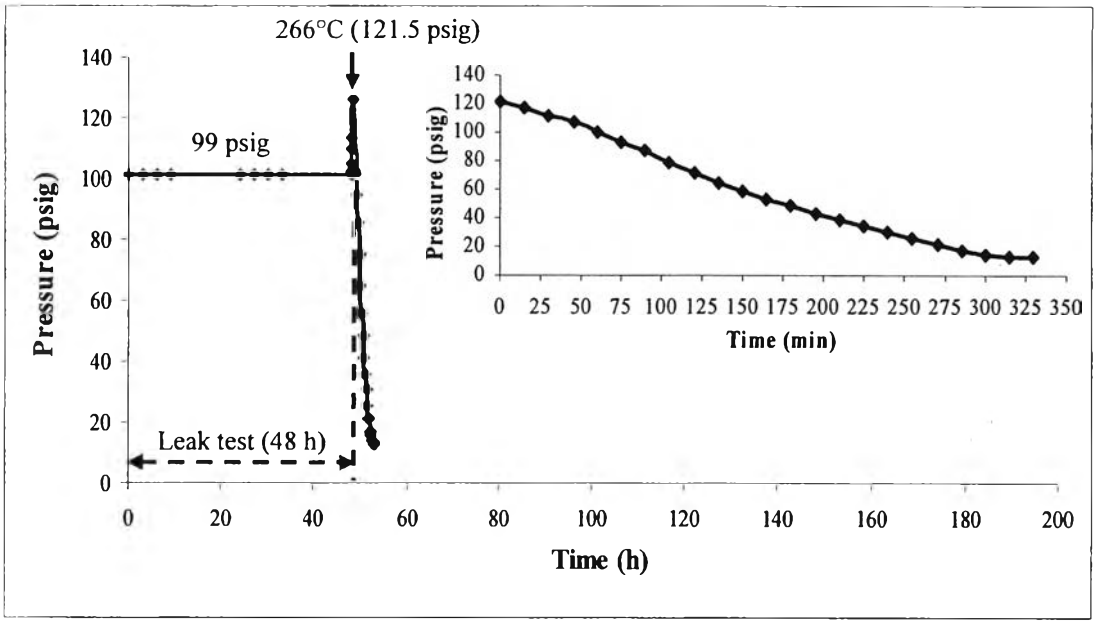

(a) Initial hydrogen pressure: 99 psig at 25°C. Set point temperature: 300°C. Tube temperature: 266°C.

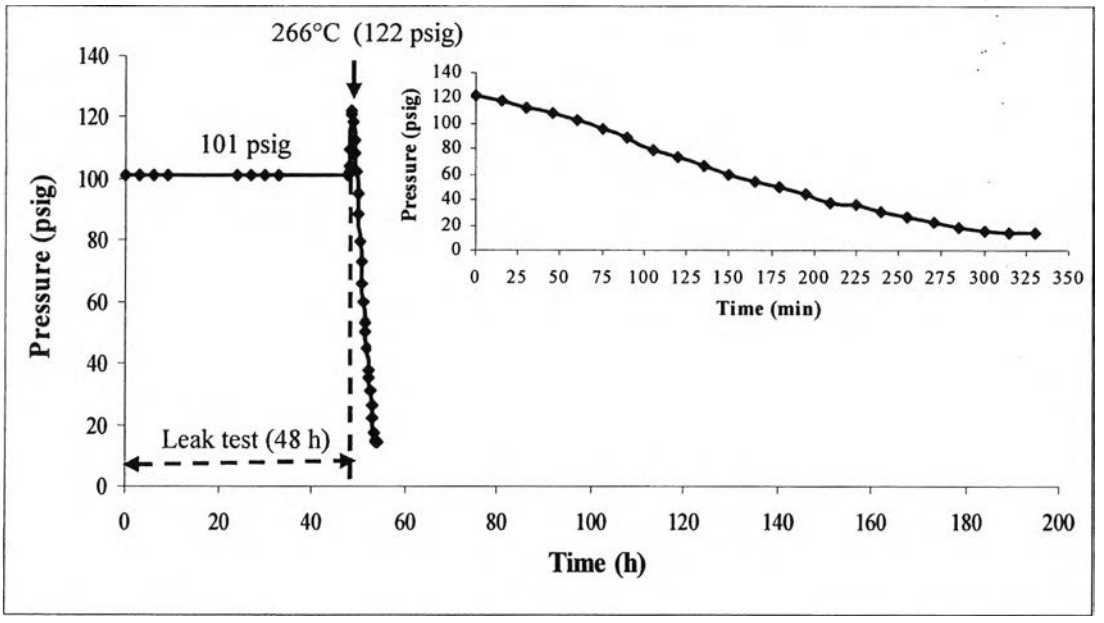

(b) Initial hydrogen pressure: 101 psig at 25°C. Set point temperature: 300°C. Tube temperature: 266°C.

Figure 4.17 The change in hydrogen pressure inside the filmed carbon steel tube with time (platinum on both the inside and outside surfaces of carbon steel tube).

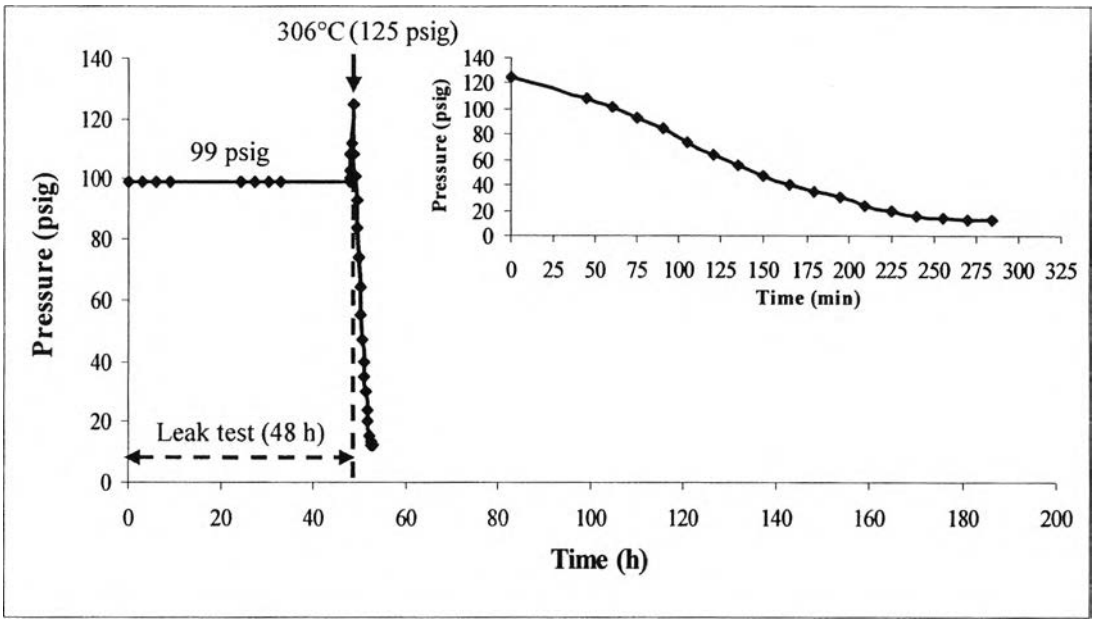

(a) Initial hydrogen pressure: 99 psig at 25°C. Set point temperature: 345°C. Tube temperature: 306°C.

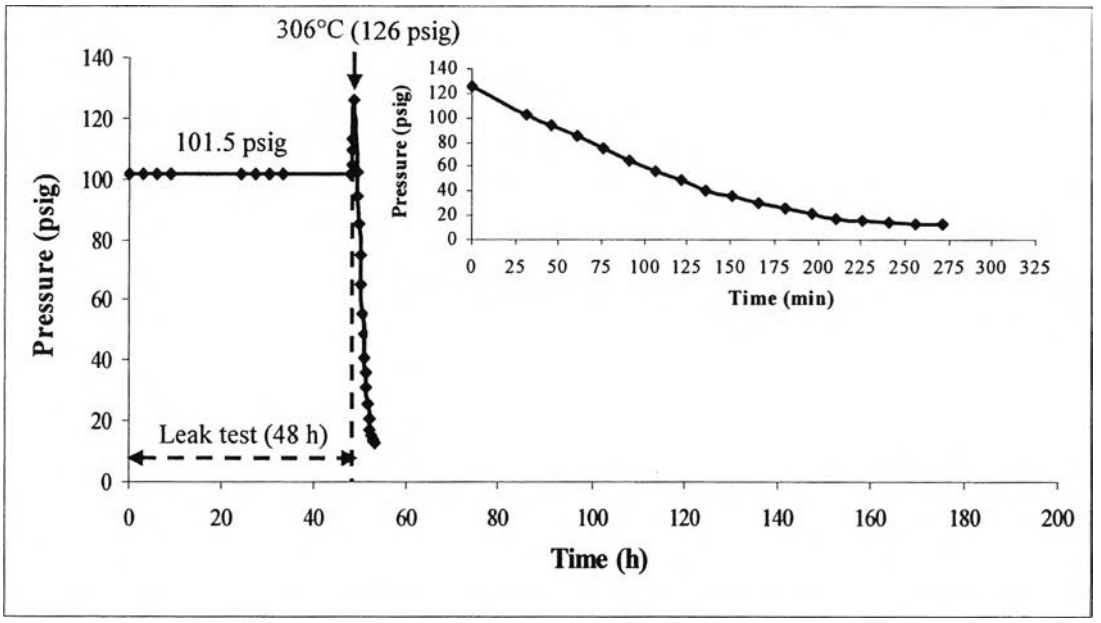

(b) Initial hydrogen pressure: 101.5 psig at 25°C. Set point temperature: 345°C. Tube temperature: 306°C.

Figure 4.18 The change in hydrogen pressure inside the filmed carbon steel tube with time (platinum on both the inside and outside surfaces of carbon steel tube).

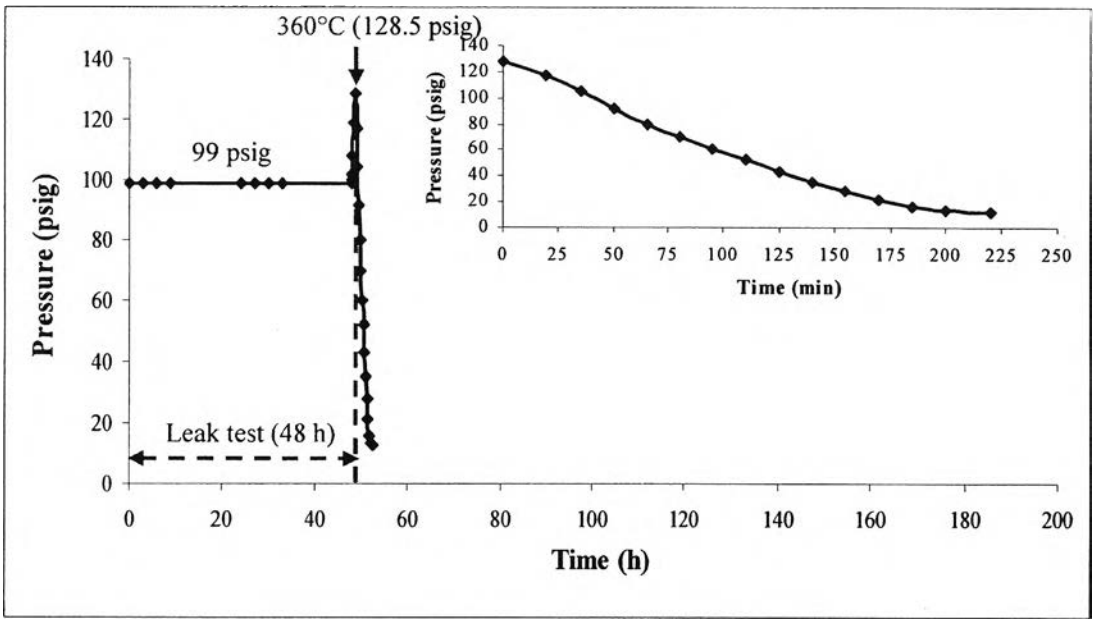

(a) Initial hydrogen pressure: 99 psig at 25°C. Set point temperature: 385°C. Tube temperature: 360°C.

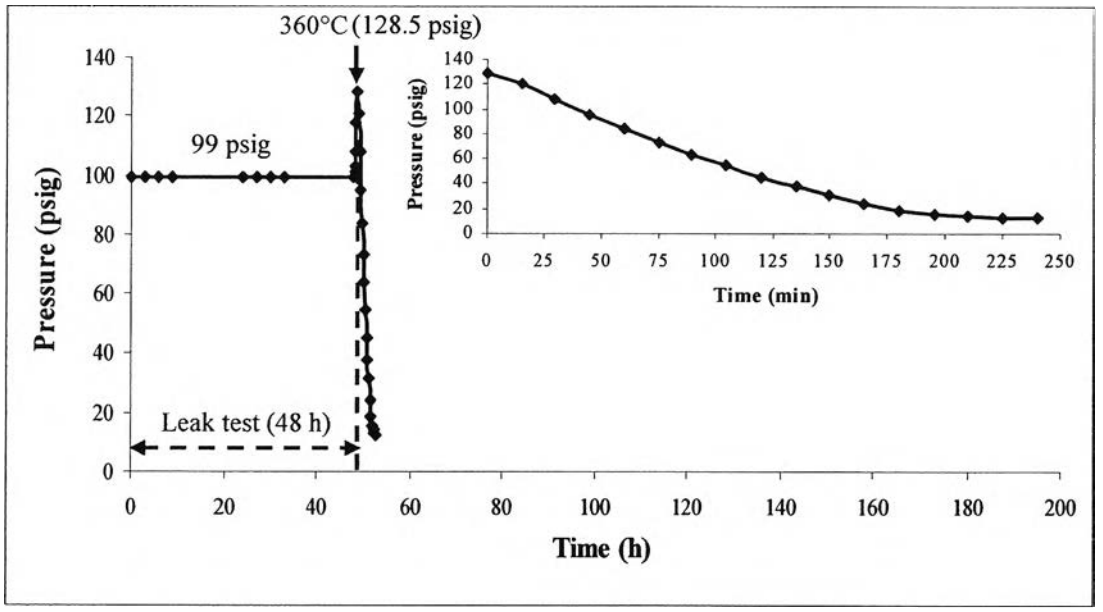

(b) Initial hydrogen pressure: 99 psig at 25°C. Set point temperature: 385°C. Tube temperature: 306°C.

Figure 4.19 The change in hydrogen pressure inside the filmed carbon steel tube with time (platinum on both the inside and outside surfaces of carbon steel tube).

The results revealed that coating platinum on the carbon steel tube surface significantly decreased the resistance to hydrogen permeation. By subtracting the difference in measured permeation caused by coating first one surface and then the other, the resistance can be estimated. Table 4.6 presents the average resistance of the carbon steel tube, the average outside and inside resistances on the carbon steel surface in this study. The average resistance of the carbon steel tube itself based on the hydrogen diffusivity is $1.58\times10^{6}\pm7.78\times10^{4}$ s/m. The surface resistances are $3.85\times10^{5}\pm9.19\times10^{3}$ s/m and $3.17\times10^{5}\pm4.45\times10^{4}$ s/m for the outside and inside surface, respectively. The resistance of a feeder pipe in the plant was determined using the measured hydrogen diffusivity in this study. The resistances of a feeder pipe in the plant are 7.10×10^{6} s/m and 5.92×10^{6} s/m for 6 mm of the wall thickness and 5 mm of the wall thickness, respectively. It can be seen that the resistance of a feeder pipe in the plant is greater than that of the carbon steel in this study because the tube wall of a feeder pipe in the plant is thicker. In addition, the response time for hydrogen diffusion through the carbon steel based on the measured hydrogen diffusivity is 40.37 minutes.

The calculated hydrogen diffusivity in nickel-alloy (Hastelloy-C) and bare carbon steel tube outside the furnace replaced by the copper tube are $2.97\times10^{-12}\,m^2/s$ and $2.32\times10^{-11}\pm7.78\times10^{-13}\ m^2/s$ at 306°C of tube surface temperature inside the furnace, respectively as shown in Table 4.7. These calculations rely on the assumption that the inside and outside resistance on the nickel-alloy and bare carbon steel surfaces are equal to that on the platinum-filmed carbon steel tube surface.

Table 4.6 Inside and outside resistance on carbon steel surface

Description	Furnace temperature (°C)	Tube temperature (°C)	Initial hydrogen pressure (psig)	Hydrogen pressure after heating (psig)	Hydrogen pressure at end of run (psig)	Resistance on carbon steel surface (s/m)
Pt coated on both the inside and outside surfaces: 1 2	 345 345	 306 306	 99 100	 125 126	 12 12.5	Tube resistance: 1.52×10^{6} 1.63×10^{6} Avg: $1.58\times10^{6} \pm 7.78\times10^{4}$
Pt coated on the inside surface: 1 2	 345 345	 306 306	 100 98	 125 123	 12.5 12.5	Outside resistance: 3.98×10^{5} 3.72×10^{5} Avg: $3.85\times10^{5} \pm 9.19\times10^{3}$
Pt coated on the outside surface: 1 2	 345 345	 306 306	 99 100	 124 124	 13.5 13.5	Inside resistance: 2.85×10^{5} 3.48×10^{5} Avg: $3.17\times10^{5} \pm 4.45\times10^{4}$

Table 4.7 Hydrogen pressure reduction (Bare, Uncoated metal)

Description	Furnace temperature (°C)	Tube temperature (°C)	Initial hydrogen pressure (psig)	Hydrogen pressure after heating (psig)	Hydrogen pressure at end of run (psig)	Hydrogen diffusivity (m^2/s)
Nickel-alloy (Hastelloy-C) tube	345	306	99	117.0	72.0	2.97×10^{-12}
Carbon steel tube outside the furnace replaced with copper tube	345 345	306 306	99 100	125.5 126.0	12.5 13.0	2.26×10^{-11} 2.37×10^{-11} Avg: $2.32\times10^{-11} \pm 7.78\times10^{-13}$

Figure 4.20 shows the influence of temperature on the hydrogen diffusivity of carbon steel tube coated with platinum on both the inside and outside surfaces (presumably with surface effects absent). It was observed that the average hydrogen diffusivity increased from $4.97\times10^{-10} \pm 2.05\times10^{-11}$ m^2/s through $6.45\times10^{-10} \pm 1.70\times10^{-11}$ m^2/s, $8.44\times10^{-10} \pm 4.10\times10^{-11}$ m^2/s to $9.71\times10^{-10} \pm 5.59\times10^{-11}$ m^2/s as the temperature increased from 180°C to 266°C, 306°C and then to 360°C (Table 4.8).

The hydrogen diffusivity data vs. temperature was fitted using the Arrhenius relationship:

$$D = D_0 \exp\left(\frac{-E_a}{RT}\right), \tag{4.1}$$

where D_0 is a temperature-independent constant (m^2/s), E_a is the activation energy for diffusion (J/mol), R is the gas constant (J/mol.K) and T is the absolute temperature (K). Figure 4.21 shows $\ln D_{(H_2)}$ vs. $1/T$ and the linear regression fit for the data. For this study, linear regression led to $D_0 = 5.27\times10^{-9}$ m^2/s and $E_a = 9{,}010.71$ J/mol. Therefore, the hydrogen diffusivity in carbon steel tube (ASTM A179) vs. temperature can be predicted by using Equation 4.2 or Equation 4.3.

$$D_{(H_2)} = 5.27\times10^{-9} \exp\left(\frac{-9{,}010.71}{RT}\right)\frac{m^2}{s} \tag{4.2}$$

or

$$D_{(H_2)} = 5.27\times10^{-9} \exp\left(\frac{-1{,}083.80}{T}\right)\frac{m^2}{s} \tag{4.3}$$

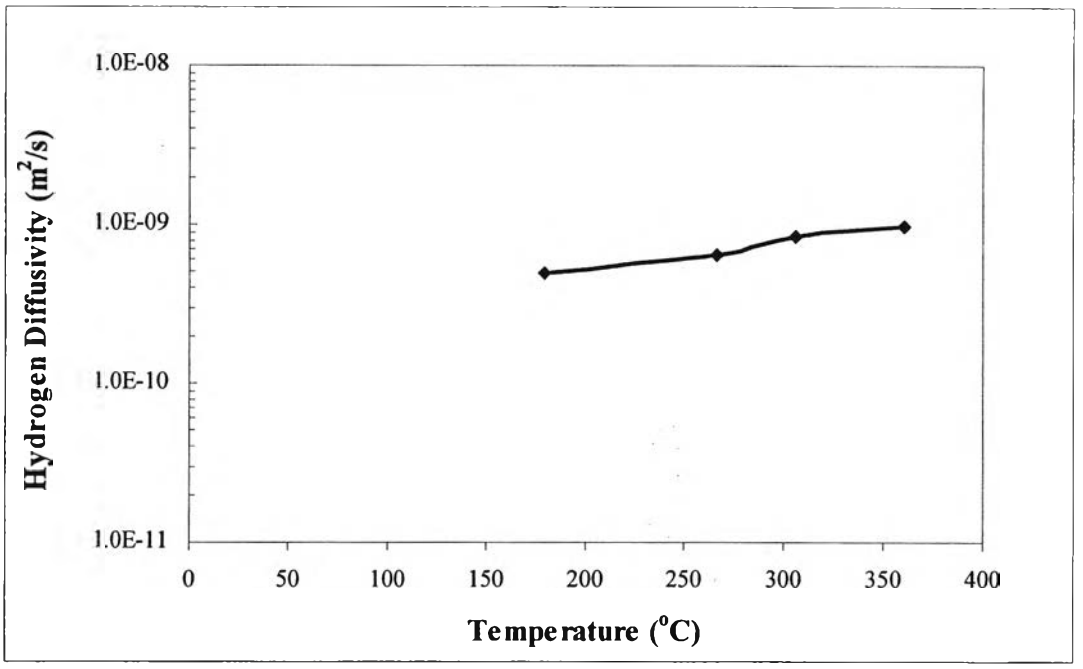

Figure 4.20 Hydrogen diffusivity evaluated as a function of temperature.

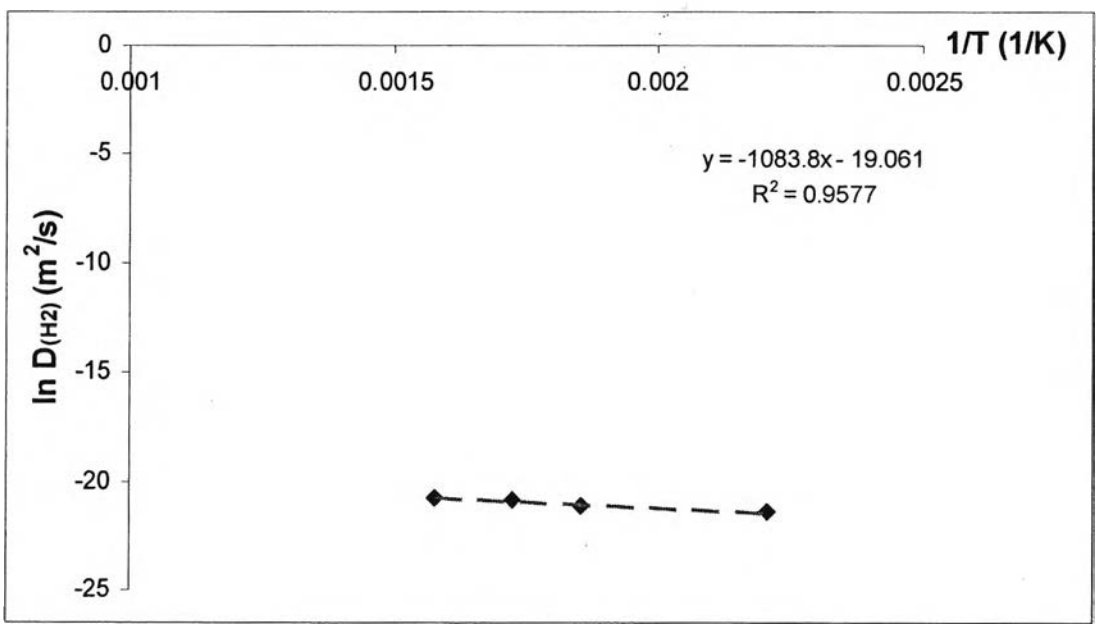

Figure 4.21 Hydrogen diffusivity evaluated as a function of reciprocal temperature.

Table 4.8 Hydrogen diffusivity in carbon steel at different temperatures

Description	Furnace temperature (°C)	Tube temperature (°C)	Initial hydrogen pressure (psig)	Hydrogen pressure after heating (psig)	Hydrogen pressure at end of run (psig)	Hydrogen diffusivity (m^2/s)
Pt coated on the inside and outside surfaces: 1 2	 215 215	 180 180	 99 99	 111.5 112	 12.5 12	 5.11×10^{-10} 4.82×10^{-10} Avg: $4.97\times10^{-10} \pm 2.05\times10^{-11}$
Pt coated on the inside and outside surfaces: 1 2	 300 300	 266 266	 99 101	 121.5 122	 12.5 14.5	 6.57×10^{-10} 6.33×10^{-10} Avg: $6.45\times10^{-10} \pm 1.70\times10^{-11}$

Table 4.8 Hydrogen diffusivity in carbon steel at different temperatures (Con't)

Description	Furnace temperature (°C)	Tube temperature (°C)	Initial hydrogen pressure (psig)	Hydrogen pressure after heating (psig)	Hydrogen pressure at end of run (psig)	Hydrogen diffusivity (m^2/s)
Pt coated on the inside and outside surfaces:						
1	345	306	99	125	12	8.73×10^{-10}
2	345	306	101.5	126	12.5	8.15×10^{-10}
						Avg: $8.44\times10^{-10} \pm 4.10\times10^{-11}$
Pt coated on the inside and outside surfaces:						
1	385	360	99	128.5	12.5	1.01×10^{-9}
2	385	360	99	128.5	12.5	9.31×10^{-10}
						Avg: $9.71\times10^{-10} \pm 5.59\times10^{-11}$

The Arrhenius equation showing temperature dependence of hydrogen diffusivity in carbon steel (ASTM A179) in this study is compared to data from the literature as shown in Figure 4.22.

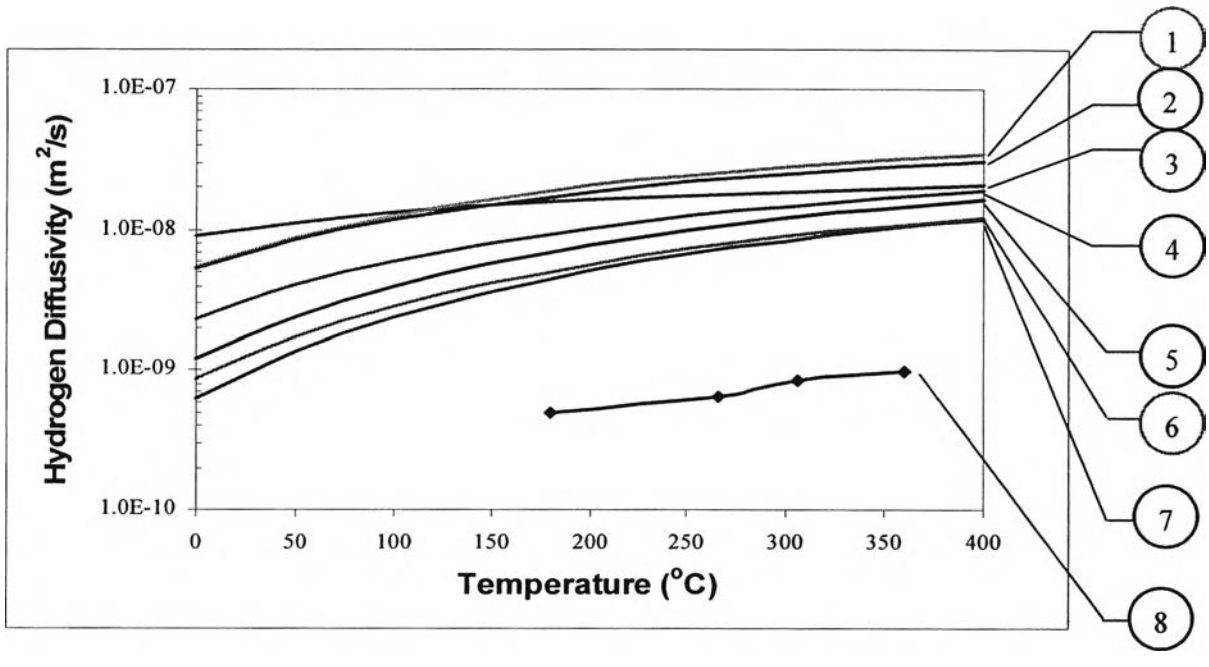

Figure 4.22 Diffusion coefficient of hydrogen in iron and carbon steel on the basis of various data: 1-from Equation (2.28), 2-from Equation (2.29), 3-from Equation (2.30), 4-from Equation (2.31), 5-from Equation (2.32), 6-from Equation (2.33) and 7-from Equation (2.34), 8-from Equation (4.3).

The Arrhenius equation data of Miller *et al.*, 1975 from equation (2.29) that used α-iron as a diffusing medium is compared with the data obtained in this work as shown in Table 4.9 due to the fact that both sides of Miller's sample were coated with palladium to eliminate the surface resistances, similarly to this study.

Table 4.9 Temperature dependence of hydrogen diffusivity in steel

Author	Types of steel	Arrhenius Equation
Miller *et al.*, 1975	α-iron: C-0.017 pct Mn-0.038 pct P-0.003 pct S-0.015 pct Si-0.004 pct Fe-balance	$D_{(H_2)} = 1.01\times10^{-7}\exp\left(\frac{-802.72}{T}\right)\frac{m^2}{s}$
This study	Carbon steel ASTM A179: *C-2.44-3.88 pct P-0.54-0.66 pct Si-0.25-0.38 pct Cr-0.09-0.15 pct Fe-balance *From EDS analysis	$D_{(H_2)} = 5.27\times10^{-9}\exp\left(\frac{-1{,}083.80}{T}\right)\frac{m^2}{s}$

The differences with the literature values may be due to the fact that data from Miller et al., 1975 were obtained using comparatively high driving pressure, more than 2,800 Pa, over a temperature range of 69 to 346°C. Furthermore, neither the inside nor the outside surface of our carbon steel tube was totally covered by platinum metal, so that surface effects might not have been eliminated entirely (in the literature, the membrane sample was completely coated with palladium metal, approximately 1000Å thick).

In addition, the hydrogen diffusivity in this study is lower than that in the α-iron might be caused by the metal-hydrogen bond. The metal-hydrogen bond for carbon steel might be higher than that for α-iron resulting in the hydrogen atoms on carbon steel will being less mobile. The decrease in hydrogen mobility could also be due to an increased blocking of interstitial sites at higher carbon contents and could be to the different grain structure, although grain boundary effects were not

part of the study. The impurity content of the carbon steel is also a possible reason i.e., trapping of hydrogen atoms by other elements as well as defects such as dislocations, inclusions, voids, etc. Also, the method of estimating diffusivity by the average rate of pressure drop over the duration of the experiment, rather than by instantaneous rates, will lead to a lower value. Therefore the difference between these two diffusion coefficients of hydrogen is reasonable.

4.5 Effect of Isotope Dependence

In the case of CANDU reactors, heavy water (D_2O) is used as a coolant in the primary heat transport system. Deuterium thus is produced as a result of flow-accelerated corrosion (FAC). The diffusion coefficient of deuterium can be estimated from the classical rate theory $D_1/D_2 = \sqrt{M_2/M_1}$ used for metal-hydrogen systems (Volkl and Alefeld, 1978), as shown in Table 4.10.

Table 4.10 Estimated deuterium diffusion coefficient

Description	Furnace temperature (°C)	Tube temperature (°C)	Hydrogen diffusivity (m^2/s)	Estimated deuterium diffusivity (m^2/s)
Pt coated on the inside and outside surfaces: 1 2	 215 215	 180 180	 5.11×10^{-10} 4.82×10^{-10} Avg: $4.97\times10^{-10} \pm 2.05\times10^{-11}$	 3.61×10^{-10} 3.41×10^{-10} Avg: $3.51\times10^{-10} \pm 1.41\times10^{-11}$
Pt coated on the inside and outside surfaces: 1 2	 300 300	 266 266	 6.57×10^{-10} 6.33×10^{-10} Avg: $6.45\times10^{-10} \pm 1.70\times10^{-11}$	 4.65×10^{-10} 4.48×10^{-10} Avg: $4.57\times10^{-10} \pm 1.20\times10^{-11}$

Table 4.10 Estimated deuterium diffusion coefficient (Con't)

Description	Furnace temperature (°C)	Tube temperature (°C)	Hydrogen diffusivity (m^2/s)	Estimated deuterium diffusivity (m^2/s)
Pt coated on the inside and outside surfaces: 1 2	 345 345	 306 306	 8.73×10^{-10} 8.15×10^{-10} Avg: $8.44\times10^{-10} \pm 4.10\times10^{-11}$	 6.17×10^{-10} 5.76×10^{-10} Avg: $5.97\times10^{-10} \pm 2.90\times10^{-11}$
Pt coated on the inside and outside surfaces: 1 2	 385 385	 360 360	 1.01×10^{-9} 9.31×10^{-10} Avg: $9.71\times10^{-10} \pm 5.59\times10^{-11}$	 7.14×10^{-10} 6.58×10^{-10} Avg: $6.86\times10^{-10} \pm 3.96\times10^{-11}$

The temperature dependence of deuterium diffusion through the carbon steel tube coated with platinum on both the inside and outside surfaces is shown in Figure 4.23. It is seen that the average estimated deuterium diffusivity increased through $3.51\times10^{-10}\pm1.41\times10^{-11}\,m^2/s$, $4.57\times10^{-10}\pm1.20\times10^{-11}\,m^2/s$, $5.97\times10^{-10}\pm 2.90\times10^{-11}\,m^2/s$ and to $6.86\times10^{-10}\pm3.96\times10^{-11}\,m^2/s$ as the surface temperature increased through 180°C, 266°C, 306°C to 360°C. These data were fitted using the Arrhenius equation to determine the activation energy for deuterium diffusion (E_a) and a temperature-independent constant (D_0).

Figure 4.24 shows the plot of $\ln D_{(D_2)}$ vs. $1/T$ and linear regression fits for the predicted values. The data at each temperature lie on straight lines for the Arrhenius plot of the deuterium diffusion. For this study, linear regression led to $D_0 = 3.72\times10^{-9}\,m^2/s$ and $E_a = 9{,}019.86$ J/mol. Therefore, the deuterium diffusivity in carbon steel tube (ASTM A179) at different temperature can be estimated by using Equation 4.44 and Equation 4.45.

$$D_{(D_2)} = 3.72\times10^{-9}\exp\left(\frac{-9{,}019.86}{RT}\right)\frac{m^2}{s} \tag{4.44}$$

or

$$D_{(D_2)} = 3.72\times10^{-9}\exp\left(\frac{-1{,}084.90}{T}\right)\frac{m^2}{s} \tag{4.45}$$

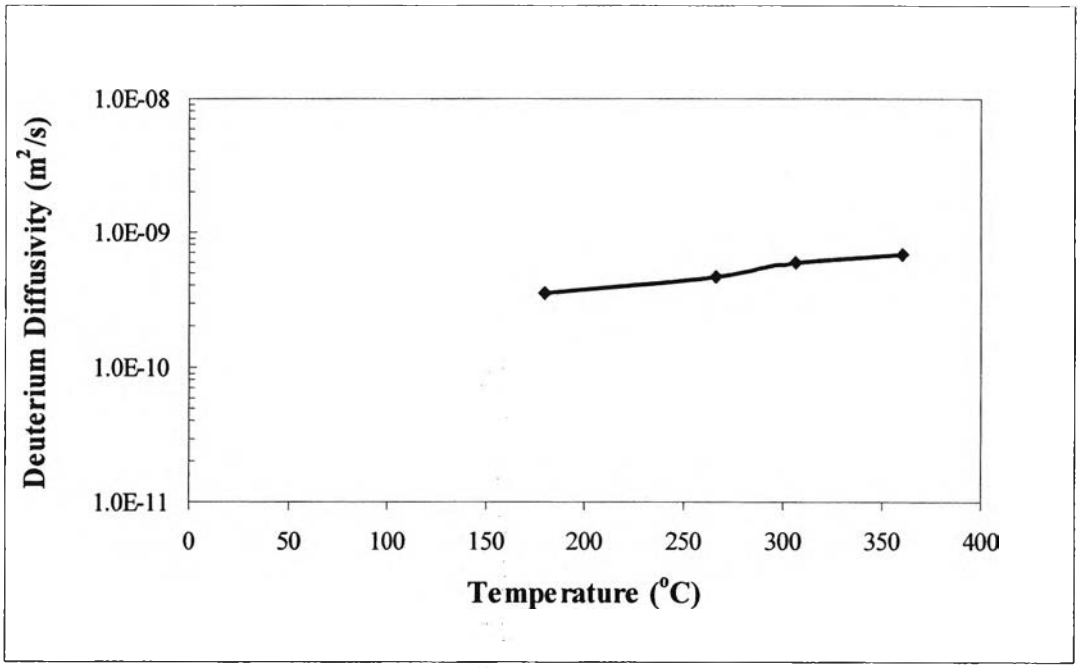

Figure 4.23 Estimated deuterium diffusivity evaluated as a function of temperature.

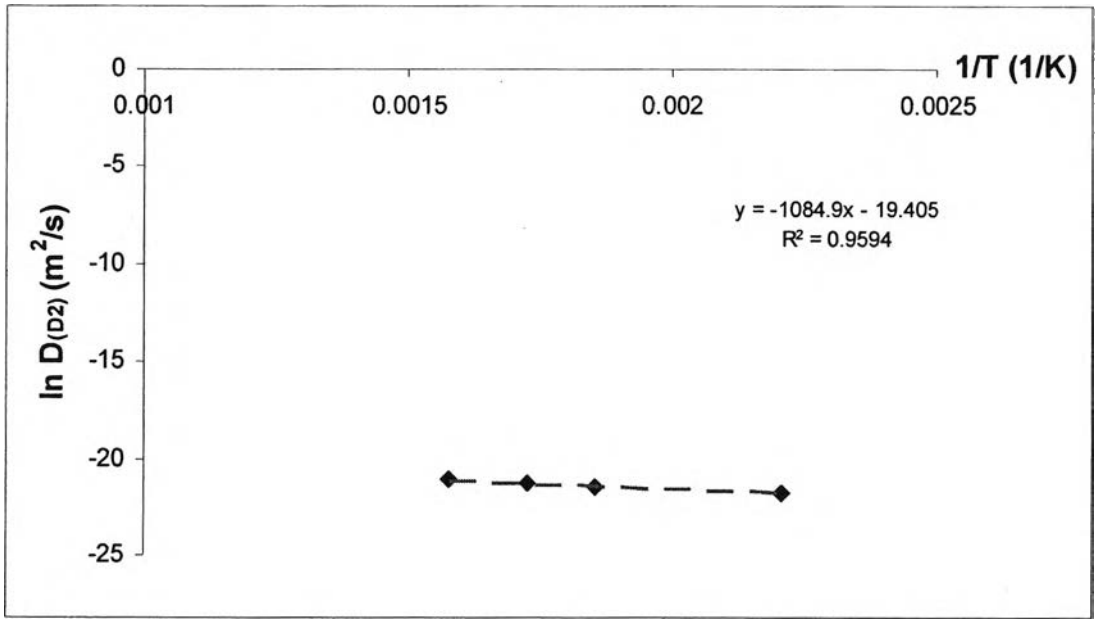

Figure 4.24 Estimated deuterium diffusivity evaluated as a function of reciprocal temperature.